Thermal Properties of Granular Silica Aerogel for High-Performance Insulation Systems

by

Adam Neugebauer

Bachelors of Science, Materials Science and Engineering
University of California, Berkeley (2004)

Submitted to the Department of Architecture
in Partial Fulfillment of the Requirements for the Degree of

Master of Science in Building Technology

at the

Massachusetts Institute of Technology

June, 2013

Signature of Author: _____
Department of Architecture
May 16, 2013

Certified by: _____
Leon Glicksman
Professor of Building Technology and Mechanical Engineering
Thesis Supervisor

Accepted by: _____
Takehiko Nagakura
Associate Professor of Design and Computation
Chair of the Department Committee on Graduate Students

Thermal Properties of Granular Silica Aerogel for High-Performance Insulation Systems

by

Adam Neugebauer

Submitted to the Department of Architecture
on May 16, 2013 in Partial Fulfillment of the
Requirements for the Degree of Master of Science in
Building Technology

ABSTRACT

Based on mounting evidence in support of anthropogenic global climate change, there is an urgency for developments in high-performance building techniques and technologies. New construction projects provide substantial opportunities for energy efficiency measures, but they represent only a small portion of the building stock. Conversely, while existing buildings are plentiful, they typically have a much narrower range of feasible energy efficiency options. Therefore, there will continue to be a need for the development of new and improved energy efficiency measures for new building construction and even more so for deep retrofits of existing buildings.

This thesis provides an overview of the research performed into the on-going development at MIT of a high-performance panelized insulation system based on silica aerogel. Two test methods were used for measuring the thermal conductivity of the granules: the transient hot-wire technique and the guarded hot-plate system. Utilizing the hot-wire set-up, it was demonstrated that compressing a bed of granules will decrease the thermal conductivity of the system until a minimum point is reached around the monolithic density of the aerogel. For the Cabot granules, this was seen at 13 mW/m-K and about 150 kg/m^3. The MIT granules showed equal performance to the Cabot granules at bed densities 20-30 kg/m^3 lower. The hot-plate testing was able to experimentally evaluate previous analytical predictions regarding the conductivity impact of the internal panel truss and the under-prediction of radiant heat transfer in the hot-wire method. Hot-wire testing was also done in a vacuum chamber to quantify potential performance improvements at reduced air pressures. Since a vacuum would require the incorporation of a barrier film into the panel system, some analyses were done into the thermal bridging potential and gas diffusion requirements of such a film. Additionally, physical prototyping was done to explore how the film would be incorporated into the existing panel design.

The aerogel-based insulation panel being developed at MIT continues to show promise, though there are still plenty of opportunities remaining in the development cycle.

Thesis Supervisor: Leon Glicksman

Title: Professor of Building Science and Mechanical Engineering

ACKNOWLEDGEMENTS

First I want to thank my advisor, Prof. Leon Glicksman, for his immeasurable help and guidance throughout my time here at MIT. I couldn't have had a better advisor. You have been the perfect fit to help me through the ups and downs, while still being ready to give me a good nudge when needed. Thank you, Leon, for inviting me to be a part of this research, which was exactly the type of project I was looking for.

I also need to thank the rest of the research team at MIT – Prof. Lorna Gibson, Kevin Chen, Prof. Gang Chen, Taofang Zeng and Yi He – and at DuPont – Dr. Vivek Kapur and Fan Li. We also were helped along the way by a couple MIT UROPs: Mary Zhuang and Delphine Kaiser. Thanks also to Ellann Cohen for an excellent passing of the baton. And thanks to the invaluable backbones of BT who managed to handle all of our urgent and always last minute requests: Kathleen Ross and Alex Golledge.

It is also important to note that this research was supported through funding by the DuPont-MIT Alliance. So thank you, DMA, for making all of this possible.

Then there's the Fraunhofer Center for Sustainable Energy Systems, which provided invaluable support for this research. Not only allowing us access to their equipment, but also their time involved in testing our samples. In particular I want to thank Kurt Roth, Nitin Shukla, Alliston Watts and Bryan Urban.

The technical support team at LaserComp was alway ready, willing and able to find an answer to my many questions. Special thanks to Andrzej Brzezinski, Kevin Collins and Akhan Tleoubaev.

Thankfully there was a long list of people that were there to help me when things went wrong, but I only have time for a few highlights. Daniel Kraemer and Ken McEnaney came to the rescue more times than I can recall. Jianjian Wang, Sungwoo Yang and Amy Marconnet all provided troubleshooting support with my equipment. I should also thank Bolin Liao and Sean Buhrmester for all of their support in the 5-004 and 3-245 labs.

When I wasn't getting help fixing things, I was probably getting help making things. I loved my times in the MIT Rapid Prototyping Shop, Woodshop and Hobby Shop. Thanks specifically to Chris Dewart, David Costanza, Richard Ong, Kristen Zeiber and Ken Stone. And a lot of this work was related to Prof. John Fernandez's prototyping class. Thanks, John, for all of your input and guidance.

My BT labmates deserve a standing ovation. I'm really going to miss you and our lunches near Steam Café. Mighty Ducts softball will always be a cherished memory.

There are a few other folks around MIT that didn't fit neatly into any of the above categories, but I don't want to miss them. Emily Ranken, Christine Sherratt, Dr. Anna Maria Coclite, Dr. Barbara Hughey, Jessica B. and Simon Howard, thank you for each of your unique contributions.

Last though anything but least, there are my friends and family. My relief valves, my sanity checks, my support staff. I wish I could thank each and every one of you but, again I must limit myself. To our wonderful cat, Tippy: thank you for constantly and incessantly reminding me that I could always take yet another break to pet you. And to my wife, Riddhi: I literally would not have made it here without you.

TABLE OF CONTENTS

LIST OF FIGURES

LIST OF TABLES

LIST OF SYMBOLS

A = Surface area of the film [m^2]

A_a = Cross-sectional area of the aerogel, normal to heat flow through the aerogel [m^2]

A_c = Cross-sectional area of the core, normal to heat flow through the aerogel [m^2]

A_e = Total cross-sectional area of the film along the edges, normal to the 1D heat flow [m^2]

A_p = Cross-sectional area of the panel (without film), normal to the 1D heat flow [m^2]

A_s = Cross-sectional area of the sample [m^2]

A_t = Cross-sectional area of the truss, normal to heat flow through the truss [m^2]

A_t' = Cross-sectional area of the truss, parallel to A_c [m^2]

A_{vp} = Cross-sectional area of the vacuum panel (with film), normal to the 1D heat flow [m^2]

c_p = Specific heat capacity of the insulation material [J/kg-K]

d_{wire} = Diameter of the hot-wire [m]

dt = Increment of time for gas diffusion [day]

dT_{corr} = Corrected value of the increase in temperature of the mid-point of the hot-wire [K]

dT_{exp} = Experimental value of the average increase in temperature along the hot-wire [K]

dT = Increase in temperature of the hot-wire [K]

eul = Euler's number = 0.577215665 [unitless]

I = Current applied to the hot-wire [A]

J = Gas transmission rate across the film [$(cm^3)_{STP}/m^2$-day-atm]

k = Thermal conductivity of the material around the hot-wire [W/m-K]

k_a = Thermal conductivity of the aerogel [W/m-K]

k_c = Thermal conductivity of the core material [W/m-K]

k_{exp} = Experimental value for thermal conductivity of the insulation material [W/m-K]

k_f = Thermal conductivity of the facing material [W/m-K]

k_N = Thermal conductivity of the test stack of N sheets [W/m-K]

k_p = Thermal conductivity of a polystyrene sheet [W/m-K]

k_s = Thermal conductivity of the sample [W/m-K]

k_t = Thermal conductivity of the truss material [W/m-K]

k_t' = Contribution to thermal conductivity of the panel by the truss [W/m-K]

l_{wire} = Length of the hot-wire [m]

L = Thickness of the film [m]

L_t = Length of a truss segment, parallel to heat flow through the truss [m]

$\dot{m}_p$ = Mass transmission rate across the film [g/m^2-day-atm]

n = Moles of gas [mol]

N = Number of sheets in the test stack [unitless]

$\dot{p}$ = Rate of internal (partial) pressure increase [atm/day]

p_{amb} = Ambient (partial) pressure [atm]

p_f = Final internal (partial) pressure (or internal (partial) pressure at "failure") [atm]

p_{int} = Internal (partial) pressure [atm]

p_o = Original internal (partial) pressure [atm]

p_{stp} = Standard (partial) pressure ≡ 0.986 (for air) [atm]

P = Permeability coefficient of the film material for a given gas [$(cm^3)_{STP}$/m-day-atm]

Q = Resistance heat generated in the hot-wire [J]

Q_{SS} = Steady-state energy flux through the sample [W]

R = Ideal gas constant ≡ 8.206x10^{-5} [m^3-atm/mol-K]

R_w = Electrical resistance of the hot-wire [Ω]

R_e = Resistance of the film along the edge, parallel to the 1D heat flow [m^2-K/W]

R_f = Resistance of the film along the face, parallel to the 1D heat flow [m^2-K/W]

R_i = Resistance of the ith element [m^2-K/W]

R_N = Resistance of the test stack of N sheets [m^2-K/W]

R_p = Resistance of the core aerogel panel, parallel to the 1D heat flow [m^2-K/W]

R_{par} = Net resistance of i elements in parallel [m^2-K/W]

R_{pi} = Contact resistance between a polystyrene sheet and an instrument plate [m^2-K/W]

R_{pp} = Contact resistance between two polystyrene sheets [m^2-K/W]

R_s = Surface resistance from the panel to the surroundings [m^2-K/W]

R_{ser} = Net resistance of i elements in series [m^2-K/W]

R_{eff}^{1D} = Net resistance of the panel system assuming 1D conduction only [m^2-K/W]

R_{eff}^{2D} = Net resistance of the panel system assuming complete 2D conduction [m^2-K/W]

t = Time since the current was applied [sec]

t_p = Panel lifetime [day]

t_{ref} = Reference time [sec]

T_C = Steady-state temperature of the cold-side plate [K]

T_H = Steady-state temperature of the hot-side plate [K]

T_{int} = Internal temperature of the panel [K]

T_{stp} = Standard temperature ≡ 273.15 [K]

V_{int} = Effective volume of gas inside the panel [m^3]

$\dot{V}_{stp}$ = Volumetric flow rate across the film, at STP [$(cm^3)_{STP}$/day]

w_c = Thickness of the core [m]

w_f = Thickness of a single panel facing [m]

w_N = Total thickness of the test stack of N sheets [m]

w_p = Thickness of a single polystyrene sheet [m]

w_s = Thickness of the sample [m]

ΔT = Steady-state temperature split across the sample [K]

θ = Angle between the panel facing and the truss [degrees]

ρ = Gas density at ambient temperature and pressure [g/m^3]

ρ_{ins} = Density of the insulation material [kg/m^3]

φ = Correction factor [unitless]

$\emptyset_a$ = Volume fraction of aerogel in the core [unitless]

$\emptyset_e$ = Cross-sectional area fraction of the film along the edge, normal to the 1D heat flow [unitless]

$\emptyset_i$ = Cross-sectional area fraction of the ith element in parallel [unitless]

$\emptyset_p$ = Cross-sectional area fraction of the core aerogel panel, normal to the 1D heat flow [unitless]

$\emptyset_t$ = Volume fraction of truss in the core [unitless]

1 BACKGROUND

The push for ever-more-efficient buildings (both new and existing) continues to be driven by various carrots and sticks in the industry. Building standards, energy codes and emission regulations all continue to raise the bar for the minimum performance of buildings while government incentives, utility rebates and market differentiation encourage projects to go above and beyond these baselines. These drivers have been seeing increased attention and urgency in the face of mounting evidence in support of anthropogenic global climate change. Therefore the industry needs to match this pace with developments in high-performance building techniques and technologies.

Since new construction provides an array of energy efficiency opportunities that may not be feasible – or in some cases even possible – in existing buildings, these new building projects often represent the low-hanging fruit for energy efficiency potential in the building market. The up-front construction costs in buildings are also relatively small in comparison to the operation and maintenance costs over their lifetime, further encouraging the implementation of energy efficiency features prior to construction. On the other hand, however, new construction represents only a small fraction of the building stock. For example, as of 2010 the total building stock in the United States was approximately 275 billion square feet. In a typical year, the United States adds approximately 5 billion square feet of new buildings, which is less than 2% of the market. Apparently a similar amount of the existing building stock is renovated each year.[1] Therefore, there will continue to be a need for the development of new and improved energy efficiency opportunities in both new building construction (to achieve zero net energy and other high-performance targets) and existing buildings (to perform deep energy retrofits).

Energy use from building operation continues to be dominated by space heating and cooling loads. According to the latest Department of Energy research, space conditioning represents about half of building energy consumption in the United States (see Figure 1.1).[2] The two main ways to minimize this source of energy consumption are to reduce the heating and cooling loads on the building and to meet these loads with more efficient heating, ventilating and air-conditioning (HVAC) systems. The former can be addressed with a higher-performance thermal envelope, including higher-performance thermal insulation.

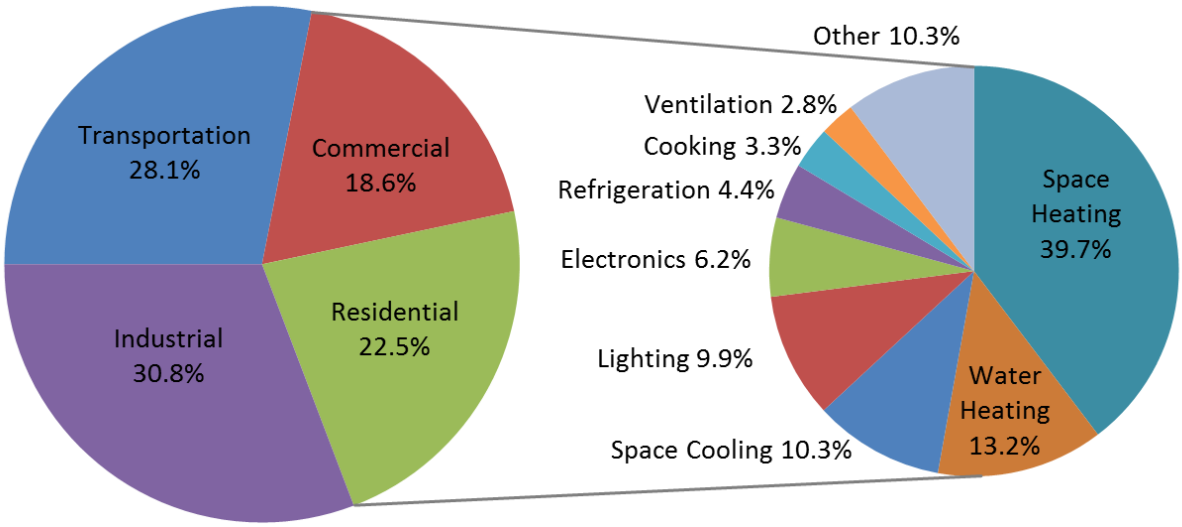

Figure 1.1: Energy use break-down by sector (left) and end-use in buildings (right).[2]

Over the history of building construction, a wide variety of materials have been utilized for thermal insulation, ranging from naturally-occurring materials (e.g., hay bales) to highly-engineered systems (e.g., vacuum insulated panels or VIPs). The primary measure of the performance for insulation products is the level of thermal insulation (known as the R-value) provided for a given thickness (typically per inch of material, in the United States). The higher the R-value per inch of an insulation product is, the better insulated a building can be or the less insulation that will be required to meet the needed performance level. Figure 1.2 provides a comparison of the more typical insulation materials used in the building industry today along with some cutting-edge products, including a monolithic silica aerogel developed and tested at MIT. Two VIP systems have also been included for comparison, though they are insulation systems rather than single insulation materials.

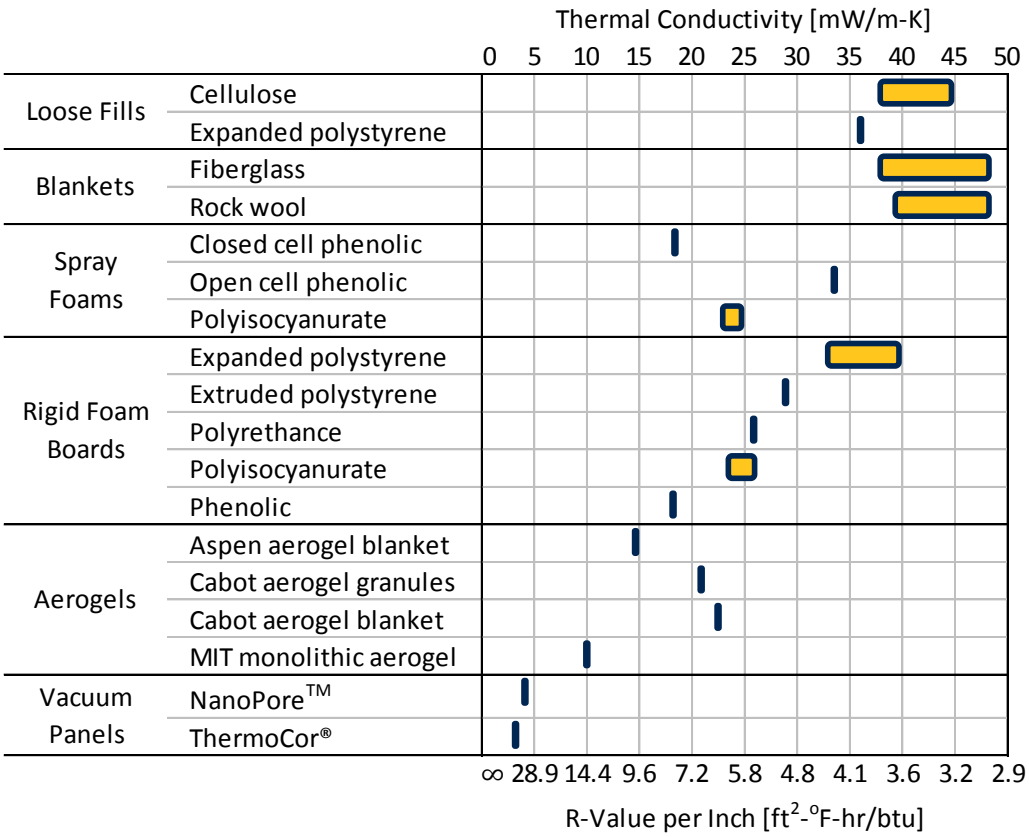

Figure 1.2: Thermal conductivity performance of various insulation materials.[3][4][5][6][7][8][9]

1.1 Aerogels as Thermal Insulation

One of the up-and-coming materials that has shown great potential for opening a new range of insulation performance is aerogel. Aerogels were first developed by S. S. Kistler in 1932 allegedly based on a bet made with fellow scientist, Charles Learned, to successfully replace the liquid in a gel with air without collapsing the solid gel network.[10] Kistler was able to do so by elevating the temperature and pressure of the sol-gel (i.e., the gel in liquid) and then carefully cooling it past its critical point (see Figure 1.3).[11]

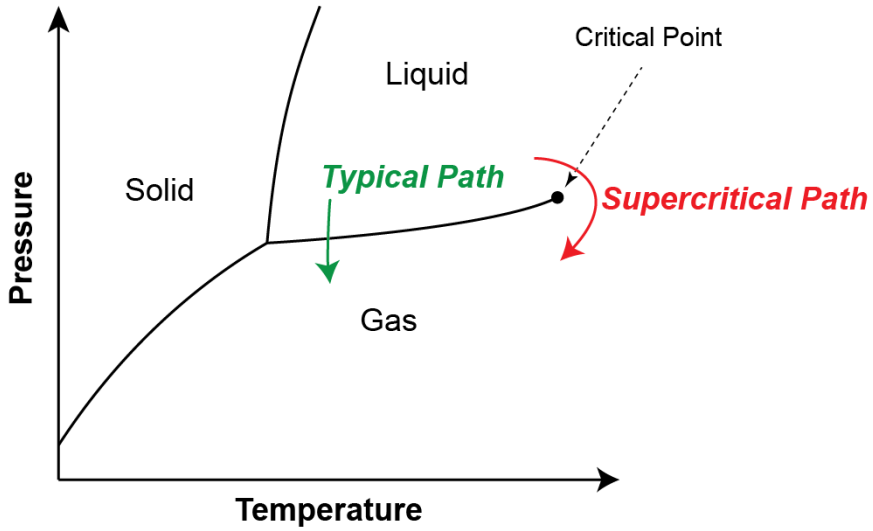

Figure 1.3: Phase diagram demonstrating supercritical drying.[3]

In 1934, Kistler documented one of the first properties of this new material: its extremely low thermal conductivity.[12] Aerogels used for thermal insulation – such as Kistler's – are often based on a silica gel, though alternative base materials have also been investigated.[13] Similarly, depending on the formulation and the synthesis process(es) relied upon, one can achieve aerogels with widely differing properties and applications: from supercapacitors to claddings for optical fibers, from a catalyst to a chemical absorber, from stellar dust collectors to anti-matter detectors.[11] The typical microstructure of aerogels has been likened to "beads on a string": semispherical particles connected by fine strands; these "strings" are interlinked, creating a fine gel structure with nanometer-scale pores. All of the applications listed above take advantage of the properties of aerogels derived from this structure: low density, high porosity and high surface area.

To understand how these properties result in low thermal conductivity, a basic understanding of heat transfer through insulation products is required. Heat transfers from one object, surface or substance to another in three main ways: conduction, convection and radiation. Conduction is the heat flow through solid material(s) or motionless fluid(s). Convection is the heat flow due to fluid motion. Finally, radiation is heat flow from one surface to another through air (or gas or vacuum) via the exchange of electromagnetic radiation. Conduction is minimized for a given material by reducing the cross-sectional area of solid in the material (as solids typically have higher thermal conductivities than fluids), which is why most insulations have relatively low densities. The remainder of the insulation is filled with air (or some other gas), which is susceptible to convection and radiation. With large air gaps,

these two mechanisms can provide much higher heat transfer than solid conduction. Large voids allow radiation to quickly bypass significant lengths of the solid material and also allow for the formation of convection currents. Therefore to minimize these heat transfer modes, the air (or gas) should be contained in small pockets or voids throughout the material; this is why most insulation materials are designed to have micro-porous structures. Additionally, conduction through the gas will be limited by the voids if the void size is on the order of the mean free path of the gas or smaller. Insulation materials can also decrease the heat transfer through the air within the pores by replacing it with a lower conductivity gas (such as argon), by decreasing the air pressure inside the insulation (such as with vacuum insulated panels) or by decreasing the emissivity of the solid material (to slow the rate of radiative heat flow).[14]

Aerogels take these same conductivity-reducing principles that are used in everyday insulation products, but push them to a new level: an aerogel's extremely low density minimizes conduction through its solid gel network and its nano-sized pores prevent the development of convection cells, reduce the rate of radiation transfer through the network and limit the conduction by the gas molecules within the pores. This research also investigated the thermal performance of aerogels in a vacuum.

1.2 Aerogel Synthesis

There are two main challenges that are faced by aerogels for use as thermal insulation. The first is to reduce the energy/material/time/cost intensity of the manufacturing process. The second challenge is to obtain a material with low thermal conductivity and sufficient mechanical strength. Both of those properties are highly dependent on the structure of the aerogel and therefore are interdependent with the first challenge. Unfortunately, improvements of one property typically come at the detriment of the other: in general, the mechanical strength of the aerogel is improved with a thicker, more robust solid silica network while lower thermal conductivity requires a finer, thinner, lower volume percent network with smaller pores. In other words, while lowering the density of the aerogel typically decreases its thermal conductivity, it also will tend to lead to decreased mechanical integrity.

These aerogel properties are affected by the manufacturing process, which can be broken down into two main stages: synthesis and aging of the sol-gel and drying of the sol-gel into an aerogel. The sol-gel synthesis and aging processes are where the structure of the solid gel network is determined; the drying process mostly impacts the quality of the final aerogel product. The synthesis procedure is often

a multi-step process where various chemical compounds are mixed in order to obtain the solid gel network in a liquid bath. For example, a typical recipe for silica aerogels uses either tetraethyl orthosilicate (TEOS) or tetramethyl orthosilicate (TMOS) as the precursor for the gel. This is then mixed with specific reagents and catalysts to cause the three synthesis reactions – hydrolysis (preparation of silica hydroxides from the precursor), condensation (combining silica hydroxides into silica oxide chains) and gelation (cross-linking of the silica oxide chains into a solid network) – in order to produce the silica gel in a solution of ethanol or methanol. See Table 6.1 in the Appendix for a list of chemicals used for the synthesis of the MIT aerogel used in this research. This is followed by an aging step to finalize the cross-linking and flush out as much of the remaining synthesis products as possible from within the gel. Additional surface treatments can also be applied at this point, such as to provide hydrophobicity (silica aerogels are naturally hydrophilic and water absorption can increase the material's thermal conductivity).

In the final stage of synthesis, the liquid solution is carefully dried in order to preserve the structure of the solid gel. Typically this is done in a process called supercritical drying. The sol-gel is placed in an autoclave and the pressure and temperature inside the chamber are gradually increased. Due to the potential danger of having a flammable organic solvent at these conditions, there is an optional solvent exchange step in which the original solvent is flushed out with carbon dioxide. In addition to being non-flammable, CO_2 also boasts a critical point with a much lower temperature than the typical organic solvents: 31^{o}C at 7.4 MPa compared to 241^{o}C at 6.3 MPa for ethanol. Once the solvent has achieved its supercritical state (in which the liquid and gaseous phases are indistinguishable), the chamber is carefully brought back to room conditions while avoiding the critical point (see the graphical representation in Figure 1.3) in order to safely bring the solvent into its gaseous state. The chamber is then opened and the aerogel is removed. If the solvent in the sol-gel was instead allowed to evaporate normally, the liquid-to-gas phase change occurring inside the pores of the gel would rupture its structure. Research has been done to find subcritical drying methods that produce useable aerogels, but those will not be discussed here since the MIT aerogel formulation uses the supercritical drying method.[11][15]

1.3 Aerogel Insulation Products

Thermal insulation products based on aerogel are already commercially available. The two largest manufacturers – Aspen Aerogels and Cabot Corporation – produce a number of different forms

of aerogel insulation, including aerogel granules, aerogel-impregnated blankets, aerogel-filled windows, coatings and paints and hybrid spray-foam systems.[5][6] While the largest markets for these aerogel insulation products continues to be industrial applications (such as subsea pipelines and cryogenic containers), there has been some limited penetration into the buildings market. In particular, the building retrofit market can be an attractive application since most methods of insulation retrofits using traditional insulation products are very invasive, time-consuming and/or space-intensive; aerogel blankets, on the other hand, can be quickly installed and provide decent insulation value without taking up significant interior volume (due to their high R-value per inch). In most cases, however, aerogel products are not a cost-competitive alternative to traditional insulation materials.

1.4 Previous Research at MIT

As part of the DuPont MIT Alliance (DMA), research began in 2009 to develop a higher-performance, cost-effective insulation product based on aerogels. This research has been conducted in parallel and in coordination with a team at DuPont led by Dr. Vivek Kapur. The MIT team has focused on silica aerogels while DuPont has been investigating alternative base materials, including organics.

The first research goal for the MIT team was to develop a new silica aerogel formulation and synthesis process. This task was initially led by graduate student Yanjia Zuo and, upon graduation, taken over by Yi He. Their efforts produced a 3-step sol-gel synthesis process based on a TEOS/ethanol formulation followed by supercritical drying with a CO_2 solvent exchange. This silica aerogel demonstrated reduced shrinking, improved mechanical properties and very low monolithic thermal conductivity (down to 9 mW/m-K at ambient conditions).[16] Yi He also identified means to reduce the duration of both the sol-gel synthesis and the CO_2 solvent exchange processes, which typically can be very time-consuming as they are diffusion-limited processes.

The second research goal for the MIT team was to develop a design for a panel system that would eventually hold the aerogels being produced. The panel would need to provide structural integrity in order for the system to withstand the expected wear-and-tear experienced in the field. However, since the panel material would have a higher thermal conductivity than the aerogel, this first goal would have to be achieved while minimizing the panel material's impact on the thermal conductivity of the insulation panel as a whole. Thomas Goutierre developed an internal pyramidal truss design made from thin polystyrene sheets that should theoretically only contribute an additional 2 mW/m-K to the conductivity of the panel core (see Figure 1.4).[17]

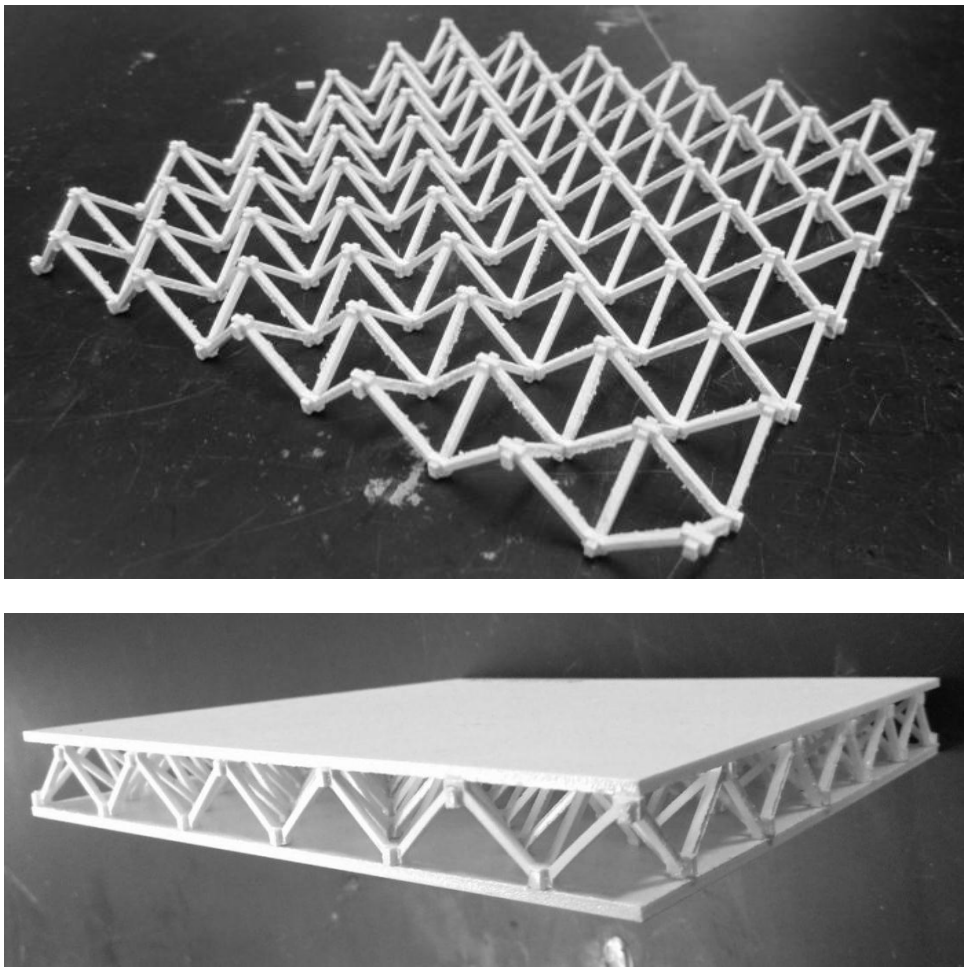

Figure 1.4: Truss system design by Thomas Goutierre, made by Kevin Chen. A constructed truss (top) and a truss installed between two panel faces (bottom).[17][18]

In parallel with these panel design efforts, Ellann Cohen developed a methodology to reliably test the thermal conductivity of the aerogel samples. Since the samples being produced were relatively small (about the size of a piece of chalk), the more traditional steady-state test methods would not work. After researching the available test methods, Cohen eventually selected the transient hot-wire method. However, due to the relatively short length of the hot-wire used for testing of the MIT samples, she also had to develop an end-effects correction for the experimental results. Additionally, Cohen found that this test method likely underestimates the thermal conductivity for the aerogel samples by up to 3.3 mW/m-K when compared to conditions that would be experienced in the field; this was due to the material's infrared transmissivity at the time and length scales relevant to this transient methodology.[3]

1.5 Summary of Thesis Research

The research covered in this thesis focused exclusively on the testing of granular silica aerogels. In addition to granules made from the MIT aerogel formulation, a commercial aerogel granule product from Cabot was also utilized for testing. See Table 6.2 in the Appendix for a comparison of the different aerogels used in this research. The work was split into two main areas: thermal conductivity testing and panel design analysis.

Chapter 2 of the thesis covers the thermal conductivity research. The hot-wire test set-up developed by Ellann Cohen and previous MIT students was again utilized, though new test chambers were made for the testing of granular materials at ambient conditions and under vacuum. A guarded hot-plate LaserComp system was also used for testing of aerogel-filled panels; this system allowed for tested of analytical results from previous research and also provided a comparison for the hot-wire results. Finally, this chapter covers some concurrent research done by Kevin Chen into the characterization of the aerogel beds under compression.

Chapter 3 reviews the research done regarding the panel design. There has been interest in developing an aerogel-filled vacuum panel, which would require the incorporation of a barrier film. Analyses were performed on the potential thermal bridging effects of such a film and the necessary diffusion barrier characteristics required of the film. Physical prototyping was also done to evaluate one method to incorporate the barrier film into the current panel design with the internal truss.

Chapter 4 draws some conclusions from the research and highlights some future research opportunities.

2 THERMAL CONDUCTIVITY TESTING

The most critical parameter of any material or panel system that comes out of the MIT aerogel research is its thermal conductivity. There are a number of other important parameters that also need to be considered (e.g., mechanical properties, sound and light transmission, material intensity, flame spread rating, manufacturing time, production cost, embodied energy, etc.), but those are secondary compared to conductivity. Therefore, thermal conductivity testing is a central portion of this research work.

Two separate techniques have been employed for thermal conductivity testing: a transient hot-wire method and a guarded hot-plate method. Each technique had its own benefits and short-comings; they also provided a level of corroboration for each other. The hot-wire method allows for the testing of small monolithic or granular samples, and a series of hot-wire tests can be completed in a matter of minutes; however, this transient method is less representative of the type of thermal conditions that an insulation material would typically experience once installed. The hot-plate method is a more traditional, steady-state test that is commonly used for evaluating insulation products; however, this test requires larger, rigid samples and a single test takes hours to run.

This chapter will describe each of these tests in more detail and then review and discuss their results. There will also be a review of some relevant physical characterization testing performed by Kevin Chen.[18]

2.1 Transient Hot-Wire Testing – Background

As mentioned in Chapter 1.4, Ellann Cohen had previously selected the transient hot-wire as the preferred test method for the aerogel samples produced at MIT. In this test, a very fine platinum wire (25.4 μm in diameter, in the MIT set-up) is surrounded by an insulation material (the aerogel) and a steady electrical current (about 65 amps, for these tests) is run through the wire for a short duration (about 1 second, for these tests). This applied current creates resistance heating in the platinum wire based on Ohm's Law (see Equation 2.1). This heat generated in the wire will cause the temperature of the wire to increase. This produces a temperature difference between the wire and its surroundings, and the heat will begin dissipating through the surrounding material. The lower the conductivity of the surrounding material, the slower the heat will dissipate from the wire and the greater the temperature of the wire will increase over time. Therefore, by measuring the temperature increase of the wire, one can calculate the conductivity of the surrounding material (see Equation 2.2) using data from the linear

portion of a hot-wire temperature versus logarithmic time plot (see Figure 2.1); experimentally, this linear fit typically has an R^2 value of at least 99.8%.[19] Equation 2.2 is derived by modeling the system as an infinite, perfectly conducting cylinder (the hot-wire) surrounded with no contact resistance by an infinite, homogenous, isotropic material (the test sample).[20]

$$Q = I{R_w}^2 \qquad \text{Equation 2.1}$$

$$k = Q/\left(4\pi \frac{dT}{dln(t)}\right) \qquad \text{Equation 2.2}$$

Where:

dT = Increase in temperature of the hot-wire [K]

I = Current applied to the hot-wire [A]

k = Thermal conductivity of the material around the hot-wire [W/m-K]

Q = Resistance heat generated in the hot-wire [J]

R_w = Electrical resistance of the hot-wire [Ω]

t = Time since the current was applied [sec]

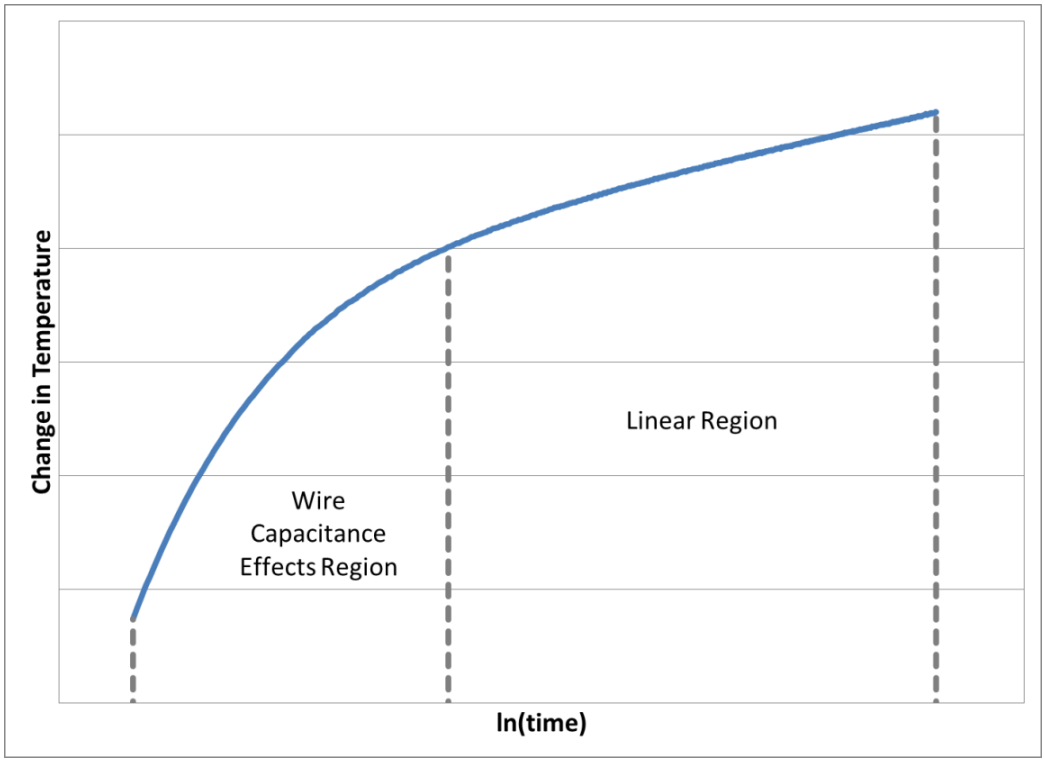

Figure 2.1: Representative plot of results from a typical hot-wire test.[3]

One issue Cohen found with this technique was that the calculated conductivity from the experimental data was dependent on the length of the wire. This effect was due to the fact that the platinum wire was being soldered to a much larger copper lead, which was acting as a heat sink. This created a gradient in the temperature along the hot-wire, when the calculations assumed it was homogenous in temperature and effectively infinite in length; therefore, the experimentally-measured temperature increase of the hot-wire is more of an average temperature increase across the length of the wire. Cohen was able to develop an analytical method to correct for this end-effect (see Equation 2.3 and Equation 2.4), which was verified with a standard reference material from the National Institute of Standards and Technologies (NIST); end-effect corrected test results for the NIST sample were within 5% of its listed conductivity value. These equations are used to calculate corrected temperatures for the mid-point along the length of the hot-wire (where the end-effects should be minimal) using the experimental results and design parameters. These corrected temperatures are then used to calculate the corrected thermal conductivity. For this technique, the experimental values are calculated using reference times of 0.5 sec and 1.0 sec and then the resulting corrected thermal conductivities based on these two reference times are averaged together to get a final thermal conductivity value.[3] This end-effect correction methodology is applied to all hot-wire test results.

$$dT_{corr} = \frac{dT_{exp}}{\left(1-\frac{1}{\varphi}\tanh(\varphi)\right)} \qquad \text{Equation 2.3}$$

$$\varphi \equiv \frac{2l_{wire}}{d_{wire}}\left[\ln\left(\frac{16k_{exp}t_{ref}}{\rho_{ins}c_p e^{eul}}\right)\right]^{-0.5} \qquad \text{Equation 2.4}$$

Where:

- c_p = Specific heat capacity of the insulation material [J/kg-K]
- dT_{corr} = Corrected value of the increase in temperature of the mid-point of the hot-wire [K]
- dT_{exp} = Experimental value of the average increase in temperature along the hot-wire [K]
- d_{wire} = Diameter of the hot-wire [m]
- eul = Euler's number = 0.577215665 [unitless]
- k_{exp} = Experimental value for thermal conductivity of the insulation material [W/m-K]
- l_{wire} = Length of the hot-wire [m]
- t_{ref} = Reference time [sec]
- ρ_{ins} = Density of the insulation material [kg/m^3]

φ = Correction factor [unitless]

Due to the transient nature of the test compared to the typical steady-state hot-plate method, Cohen discovered that this method would underestimate the contribution of radiation to the overall heat transfer within the aerogel. Based on laboratory tests into the transmissivity of aerogel, it was analytically estimated that the hot-wire tests could be underestimating the thermal conductivity of the aerogel samples compared to steady-state conditions by up to 3.3 mW/m-K.[3] Results looking into this issue will be discussed in Chapter 2.5.

2.2 Transient Hot-Wire Testing – Methods and Materials

A test chamber was constructed in order to allow for hot-wire conductivity testing of granular materials under uniaxial compression (see Figure 2.2). The hot-wire was suspended through the lower half of the chamber, which was then filled with aerogel granules. The internal dimensions of the chamber were 9.0 x 5.0 x 7.5 cm (length x width x height) and the hot-wires were installed to lengths between 7 and 8 cm. A compression plate was used to incrementally compress the granule bed after each set of hot-wire tests in order to observe the thermal conductivity behavior of the aerogel granules across a range of compression. MIT samples were tested in this way along with some commercially-available aerogel insulation granules from Cabot (product number TLD 302). This test chamber was calibrated using the same NIST reference material discussed in Chapter 2.1.

Bed density was selected as the preferred independent variable, as most others (e.g., applied pressure, compression percent or compression depth) were significantly dependent on the initial conditions and/or the chamber attributes (such as friction). Additionally, bed density is a more direct representation of the amount of material required to achieve a specific performance level. Therefore, the bed density for each test was calculated using the mass of the granules in the chamber and the internal volume of the chamber (based on the current height of the compression plate).

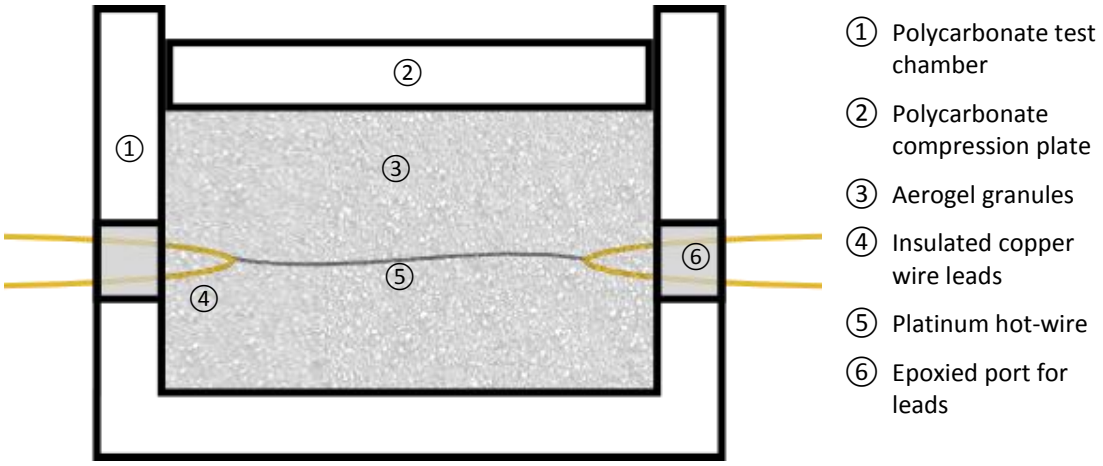

Figure 2.2: Diagram of the test chamber for the hot-wire testing of aerogel granules.

Additionally, it had been previously shown that the thermal conductivity of monolithic aerogel samples can benefit greatly from even modest levels of vacuum. However, granular samples had only undergone minimal testing in the vacuum.[3] Therefore a vacuum chamber was obtained in order to repeat these hot-wire tests across a range of bed densities but now also through increasing levels of depressurization. Due to internal dimensions of the vacuum chamber, a smaller test chamber was developed. The original test chamber design was modified to maximize its internal dimensions within the constraints of the vacuum chamber. The new test chamber had internal dimensions of 5.35 x 2.57 x 4.50 cm (length x width x height) and the hot-wires were installed to lengths between 3 and 4 cm. During the test, the leads from the test chamber would be connected to wires that led through the chamber stem to a multi-pin port on the outside of the vacuum chamber. The chamber would be depressurized with a rotary vane vacuum pump until the internal pressure was at or below the desired pressure, at which point the supply valve would be closed and the vacuum pump would be turned off. The internal pressure could then be fine-tuned with the release valve as needed (see Figure 2.3). Note that the pressure gauge was installed at a T-junction along the supply tube for the vacuum chamber. Measuring the air pressure directly within the test chamber was not feasible for these tests.

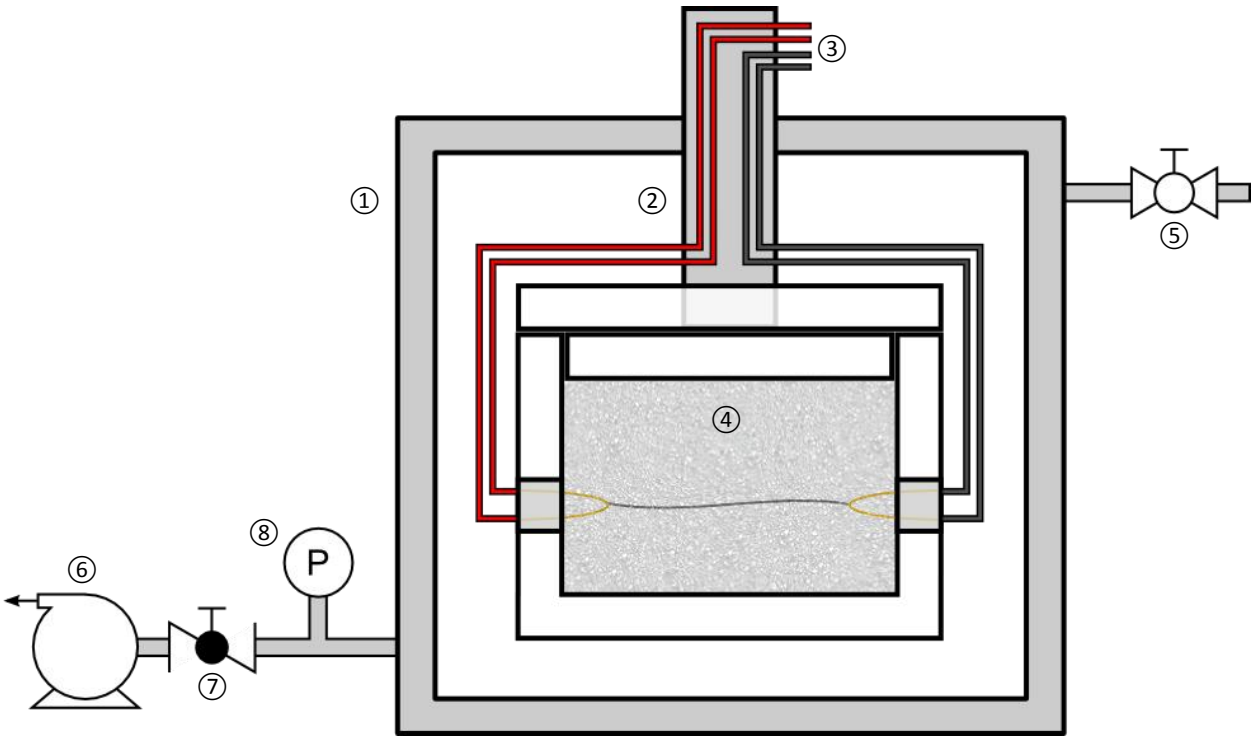

① Vacuum chamber ② Chamber stem ③ Insulated wire leads
④ Test chamber ⑤ Release valve ⑥ Vacuum pump
⑦ Supply valve ⑧ Pressure sensor

Figure 2.3: Diagram of the vacuum chamber set-up for the hot-wire testing of aerogel granules.

2.3 Transient Hot-Wire Testing – Results

Figure 2.4 shows the thermal conductivity results for MIT and Cabot granules for a range of bed densities at ambient air pressure. These results represent conductivity values after applying the end-effects correction discussed in Chapter 2.1. With no applied compression, the Cabot granules had a bed density of approximately 70 kg/m^3 and a thermal conductivity around 24 mW/m-K. The MIT granules showed a similar conductivity with no applied compression, but had a bed density around 46 kg/m^3. Upon compressing the Cabot granules, they showed a minimum conductivity of about 13 mW/m-K around 150 kg/m^3. The minimum conductivity tested for the MIT granules was about 12 mW/m-K (at 132 kg/m^3), however the minimum point was not achieved for the MIT samples before reaching the compression limits of the test chamber. For the MIT curve tested to 132 kg/m^3, the test result at 71 kg/m^3 deviated from the other MIT results at that density by about 2 mW/m-K whereas the other results

more closely agreed with the other MIT results; the reason for this discrepancy was not immediately clear without further testing.

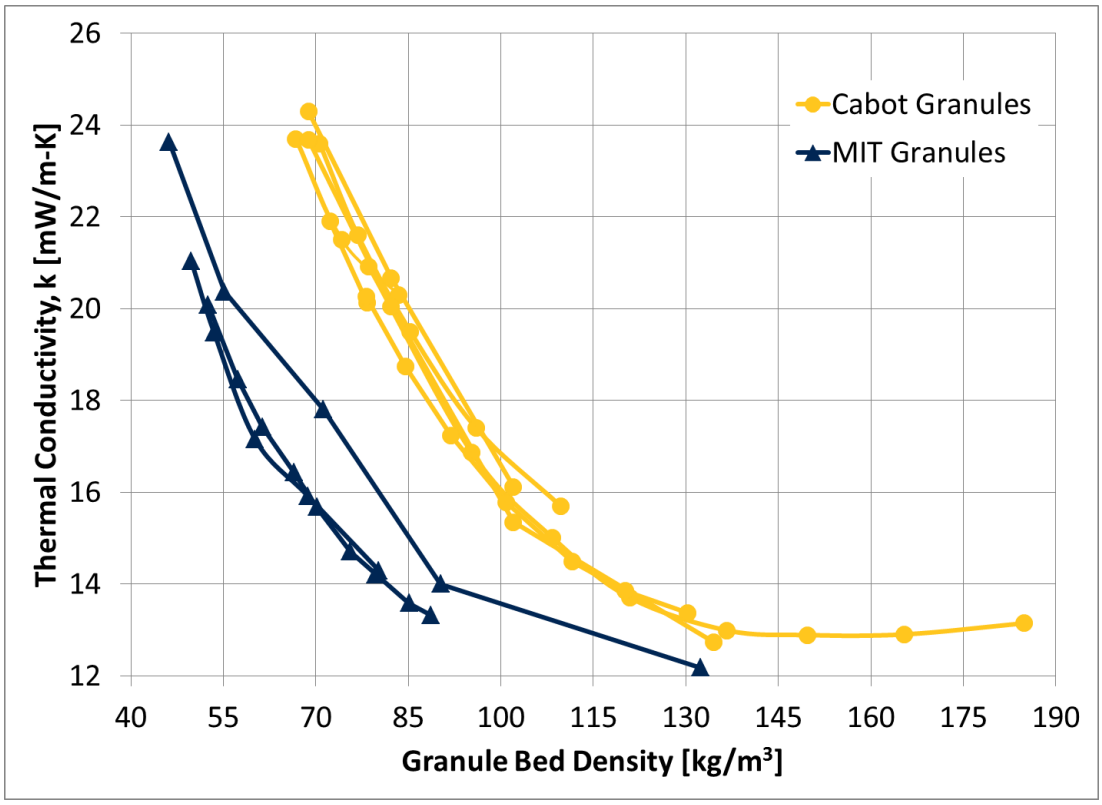

Figure 2.4: End-effect corrected thermal conductivity hot-wire test results for granular silica aerogels samples under compression.

Figure 2.5 shows the test thermal conductivity results for MIT and Cabot granules for a range of internal air pressures. Results from Ellann Cohen's testing of a monolithic MIT sample have also been included for comparison.[3] The MIT and Cabot granules demonstrated similar patterns in their thermal conductivity versus air pressure curves. They all showed the overall trend of having lower conductivities at lower air pressures, since a vacuum has a lower conductivity than air. As the air pressure decreases, the mean free path of air increases. Once the mean free path is limited by the internal pore or intergranular void size, the thermal conductivity begins to drop. For monolithic aerogel samples (with pore sizes on the order of 2-100 nm), the mean free path of air will quickly be limited and therefore the thermal conductivity will drop quickly at even modest decreases in air pressure.[3] On the other hand, a bed of granules will contain relatively large inter-granular voids in additional to the nanopores within

each granule. The granules themselves should behave similar to the monolithic samples, but the conductivity behavior of the intergranular voids will depend on their size and distribution. Based on the results from the granular samples, it appears that after an initial drop in conductivity, the slope of the granular curve is decreased from 0.50 atm until around 0.05 atm, at which point conductivity begins dropping more steeply again. The initial drop in conductivity is most likely due to mean free path being limited by the nanopores within granules and the later drop is due to the mean free path finally being reached in the inter-granular voids. At higher bed densities, the plateau effect appeared less distinct (presumably due to a decrease in the size of the inter-granular voids) and the curve appeared to more closely resemble the shape obtained from the monolithic samples. Also, below 0.01 atm it appeared that the thermal conductivities began to converge for different bed densities.

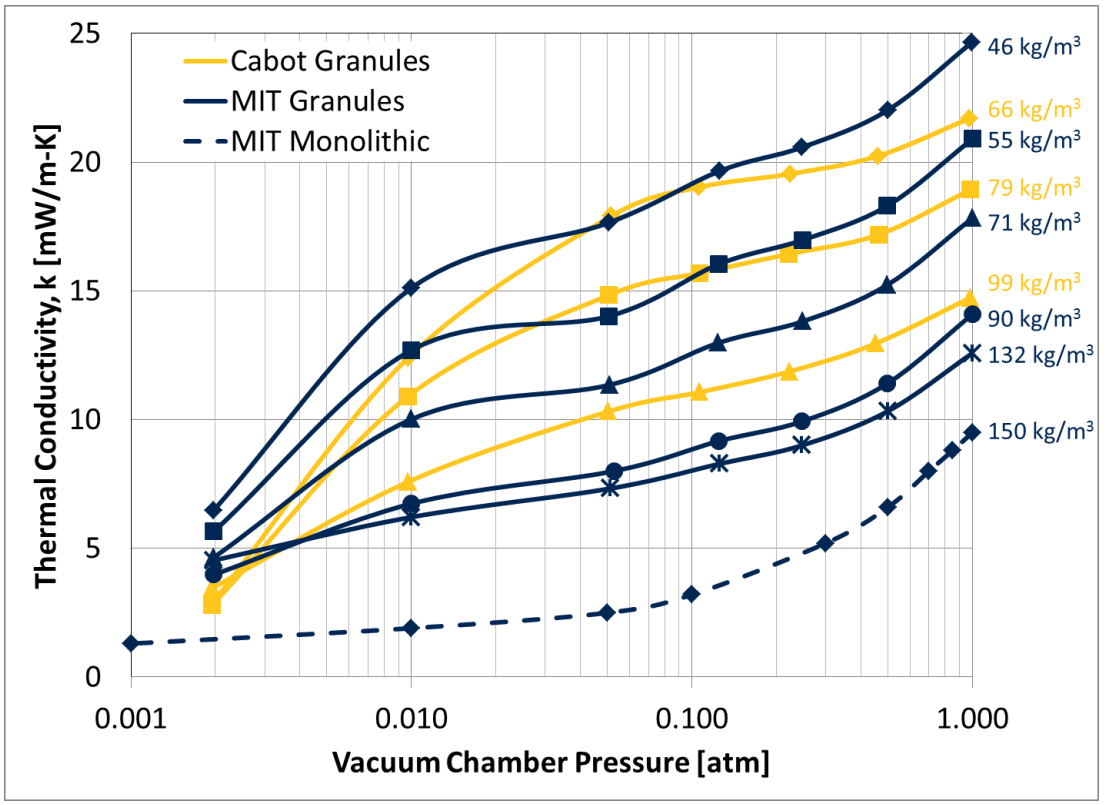

Figure 2.5: End-effect corrected thermal conductivity hot-wire test results for Cabot and MIT silica aerogel granules under vacuum compared to results by Cohen of a monolithic MIT sample.[3]

2.4 Guarded Hot-Plate Testing – Methods and Materials

As mentioned in Chapter 1.4, Thomas Goutierre previously developed a panel and truss design (see Figure 1.4) that provides the necessary mechanical integrity for an aerogel-filled panel while minimizing its contribution to the thermal conductivity of the system. Kevin Chen constructed a number of 24.7 x 24.7 x 1.9 cm (external length x width x height) panels for testing following Goutierre's design; the face and edge pieces for the panel were all made from 2 mm rigid polystyrene sheets. The thermal conductivity of these panels was then tested by the guarded hot-plate method using a LaserComp FOX304 system (with a listed accuracy of ±1%); as a precaution, a piece of foam board insulation was put around each panel to fill in the remainder of the 30.5 x 30.5 cm test chamber.[21] In this set-up, the thermal conductivity is evaluated by placing the sample between two parallel plates that are held at constant temperatures with a selected temperature split between them. Once the system has reached a thermal steady-state, the conductivity of the sample can be calculated using Fourier's Law (see Equation 2.5 and Equation 2.6). The flux flowing through the system from the hot-side plate to the cold-side plate is determined based on the energy required to hold the plates at constant temperature.

$$\frac{Q_{SS}}{A_S} = \frac{k_S \Delta T}{w_S} = \frac{k_S (T_H - T_C)}{w_S} \qquad \text{Equation 2.5}$$

$$k_S = \frac{w_S Q_{SS}}{A_S (T_H - T_C)} \qquad \text{Equation 2.6}$$

Where:

- A_S = Cross-sectional area of the sample [m^2]
- k_S = Thermal conductivity of the sample [W/m-K]
- Q_{SS} = Steady-state energy flux through the sample [W]
- ΔT = Steady-state temperature split across the sample [K]
- T_C = Steady-state temperature of the cold-side plate [K]
- T_H = Steady-state temperature of the hot-side plate [K]
- w_S = Thickness of the sample [m]

As shown above, this method provides the thermal conductivity of the sample as if it was one homogeneous material. Therefore, further calculations are required in order to determine the thermal conductivity of the core of the panel based on the experimental conductivity and design of the panel

sample. The LaserComp system is a center-of-panel design (i.e., the heat flow measurements are taken from a 10.2 x 10.2 cm metering area in the center of the chamber), so the impacts of the edge pieces of the insulation panels can be ignored.[22][21] From there, it is assumed that this experimental conductivity represents one dimensional heat flow through the sandwich panel system, with the panel core in series with the two panel faces (see Figure 2.6). Therefore the conductivity of the panel core can be calculated from the experimental conductivity of the whole panel (see Equation 2.7 and Equation 2.8).

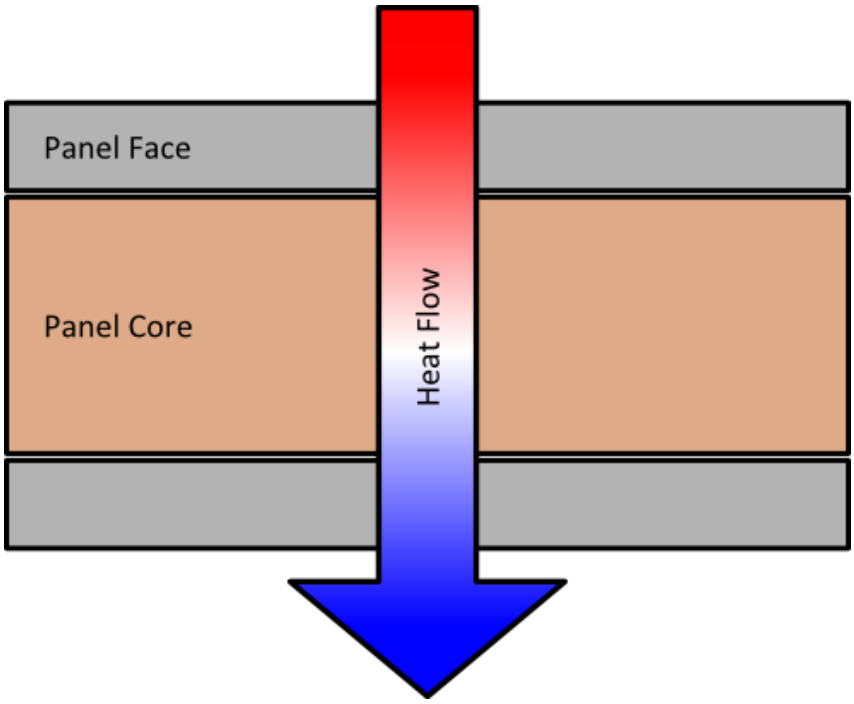

Figure 2.6: Schematic of 1D heat flow through insulation panel.

$$\frac{w_s}{k_s} = 2\frac{w_f}{k_f} + \frac{w_c}{k_c} \qquad \text{Equation 2.7}$$

$$k_c = w_c\left(\frac{w_s}{k_s} - \frac{2w_f}{k_f}\right)^{-1} \qquad \text{Equation 2.8}$$

Where:

k_c = Thermal conductivity of the core material [W/m-K]

k_f = Thermal conductivity of the facing material [W/m-K]

w_c = Thickness of the core [m]

w_f = Thickness of a single panel facing [m]

Just as with the k_s value, k_c represents the thermal conductivity assuming the core is a single homogenous material. For the insulation panels where the core has no truss, the calculated thermal conductivity of the aerogel would simply equal this k_c value. However, for the panels with a truss system, an additional calculation is required. In order to do this, we need to make the assumption that heat is conducted separately and in parallel through the aerogel and the truss (see Figure 2.7 and Equation 2.9). The thermal conductivity of the aerogel can then be determined based on this representation of materials in parallel with an additional term based on the design of the truss (see Equation 2.10).

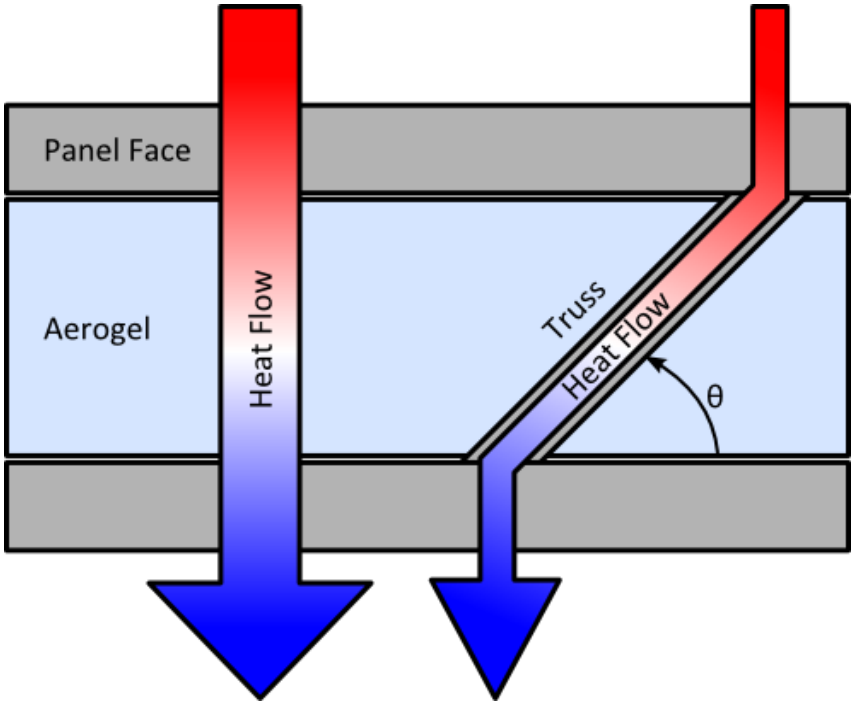

Figure 2.7: Schematic of 1D heat flow through panel core.

$$A_c \frac{k_c}{w_c} = A_a \frac{k_a}{w_c} + A_t \frac{k_t}{L_t} \qquad \text{Equation 2.9}$$

$$k_a = \frac{w_c}{A_a}\left(A_c \frac{k_c}{w_c} - A_t \frac{k_t}{L_t}\right) \qquad \text{Equation 2.10}$$

Where:

A_a = Cross-sectional area of the aerogel, normal to heat flow through the aerogel [m^2]

A_c = Cross-sectional area of the core, normal to heat flow through the aerogel [m^2]

A_t = Cross-sectional area of the truss, normal to heat flow through the truss [m^2]

k_a = Thermal conductivity of the aerogel [W/m-K]

k_t = Thermal conductivity of the truss material [W/m-K]

L_t = Length of a truss segment, parallel to heat flow through the truss [m]

Furthermore, Equation 2.8 and Equation 2.10 can be combined (see Equation 2.11), updated with a number of substitutions (see Equation 2.12) and further simplified to form a single calculation for the aerogel conductivity based on the experimental results and the panel design (see Equation 2.13). Additionally, it can be worthwhile to also determine the impact that the truss system has to the thermal conductivity of the whole panel (see Equation 2.14); as mentioned in Chapter 1.4, the truss was designed so this value would be no more than 2 mW/m-K.

$$k_a = \frac{w_c}{A_a}\left[A_c\left(\frac{w_s}{k_s} - \frac{2w_f}{k_f}\right)^{-1} - A_t\frac{k_t}{L_t}\right] \quad \text{Equation 2.11}$$

$$k_a = \frac{A_c(w_s - 2w_f)}{A_a}\left(\frac{w_s}{k_s} - \frac{2w_f}{k_f}\right)^{-1} - \frac{A_c}{A_c}\frac{A_t' \sin^2\theta\, k_t}{A_a} \quad \text{Equation 2.12}$$

$$k_a = \frac{w_s - 2w_f}{\emptyset_a}\left(\frac{w_s}{k_s} - \frac{2w_f}{k_f}\right)^{-1} - \left(\frac{1}{\emptyset_a} - 1\right)\frac{k_f}{2} \quad \text{Equation 2.13}$$

$$k_t' \equiv (\emptyset_t \sin^2\theta)k_t = k_c - \emptyset_a k_a \quad \text{Equation 2.14}$$

Where:

A_t' = Cross-sectional area of the truss, parallel to A_c [m^2]

k_t' = Contribution to thermal conductivity of the panel by the truss [W/m-K]

$\emptyset_a$ = Volume fraction of aerogel in the core [unitless]

$\emptyset_t$ = Volume fraction of truss in the core [unitless]

θ = Angle between the panel facing and the truss [degrees]

Assuming:

$A_t \equiv A_t' \sin\theta$

$$k_f = k_t$$

$$L_t \equiv \frac{w_c}{\sin\theta}$$

$$w_c = w_s - 2w_f$$

$$\phi_a \equiv \frac{A_a}{A_c}$$

$$\phi_t \equiv \frac{A_t'}{A_c} = 1 - \phi_a$$

$$\sin^2\theta = \sin^2(45°) = 0.5$$

All of these calculations are dependent upon the conductivity of the facing and truss materials (both polystyrene sheets), but the material data sheets provided by the manufacturer of the polystyrene sheets did not include values for thermal conductivity.[23] Literature research provided conductivity values for solid polystyrene of 126 and 150 mW/m-K.[24][25] This uncertainty in polystyrene conductivity could result in significant uncertainty in the calculated aerogel conductivity. Therefore, additional hot-plate tests were required to determine the polystyrene conductivity. The sheets were too thin to test on their own, so stacks of sheets were tested at once according to a thin material test methodology provided by LaserComp.[26] When stacks of sheets are tested, there will be contact resistances between the sheets (shown schematically in Figure 2.8). This situation can be represented by Equation 2.15.

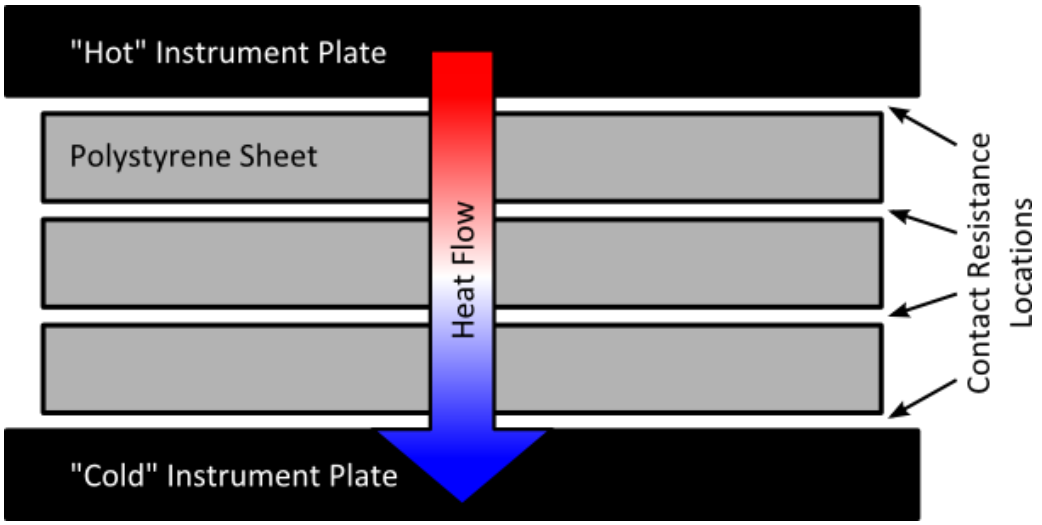

Figure 2.8: Schematic of 1D heat flow through stack of polystyrene sheets.

$$R_N = \frac{w_n}{k_n} = N\frac{w_p}{k_p} + 2R_{pi} + (n-1)R_{pp} \qquad \text{Equation 2.15}$$

Where:

k_N = Thermal conductivity of the test stack of N sheets [W/m-K]

k_p = Thermal conductivity of a polystyrene sheet [W/m-K]

N = Number of sheets in the test stack [unitless]

R_N = Resistance of the test stack of N sheets [m^2-K/W]

R_{pi} = Contact resistance between a polystyrene sheet and an instrument plate [m^2-K/W]

R_{pp} = Contact resistance between two polystyrene sheets [m^2-K/W]

w_N = Total thickness of the test stack of N sheets [m]

w_p = Thickness of a single polystyrene sheet [m]

These contact resistances cannot readily be directly quantified, so according to the LaserComp protocol multiple tests need to be completed using different numbers of sheets. These experimental results could then be plotted as the tested stack resistances versus the number of sheets. Assuming the contact resistances shown in Figure 2.8 are constant between tests, the slope of the best fit line across these points should be represented by Equation 2.16, which is derived from Equation 2.15. As long as the contact resistance between the sheets is much less than the resistance of a single sheet (i.e., $R_{pp} \ll \frac{w_p}{k_p}$), Equation 2.16 can be simplified to solve for the conductivity of the polystyrene sheets using only known values (see Equation 2.17). In order to minimize these contact resistances, a thin layer of high-conductivity thermal paste can be applied between the sheets prior to testing.

$$\frac{\Delta R_N}{\Delta N} = \frac{w_p}{k_p} + R_{pp} \qquad \text{Equation 2.16}$$

$$k_p \approx w_p / \left(\frac{\Delta R_N}{\Delta N}\right) \qquad \text{Equation 2.17}$$

2.5 Guarded Hot-Plate Testing – Results

A variety of panel configurations was tested with the LaserComp system: panels of uncompressed aerogel beds with and without a truss; panels of compressed aerogel beds with and without a truss; panels of compressed aerogels using different compression techniques; and panels of

compressed aerogels using different gluing techniques. Due to limitations in the volume of MIT granules that could be produced, all of these tests were performed using Cabot granules (product number P100). This is a different product than was used for the hot-wire testing (TLD 302) because there was insufficient TLD 302 product available and it was no longer available for purchase through Cabot. A Cabot representative stated that the TLD 302 product is the same as the current P300 product.[27] The P300 product differs from the P100 product only in terms of the particle size range (1.2-4.0 mm versus 0.01-4.0 mm, respectively), otherwise they have the same listed particle densities and thermal conductivity profiles.[6] Additionally, hot-wire testing of the P100 granules provided results similar to the TLD 302 granules. Therefore, these two products were assumed to be comparable for the purposes of this research. Again, see Table 6.2 in the Appendix for a comparison of these different aerogel materials.

Before the test results could be fully analyzed, however, the LaserComp system was also used to test the thermal conductivity of the polystyrene sheets per the method described in Chapter 2.4. The LaserComp testing of a stack of five polystyrene sheets gave a thermal conductivity for the polystyrene of 112 mW/m-K. However, attempts to test stacks of fewer sheets and attempts to minimize contact resistances with thermal paste, according to the LaserComp methodology, were both unsuccessful.

The LaserComp experimental results were then used to calculate the thermal conductivities of the aerogel beds within each test panel. Since a conclusive value could not be obtained experimentally for the polystyrene sheets, values calculated from the LaserComp results (which are dependent on the polystyrene conductivity) are provided for the lowest and highest values found: 112 mW/m-K and 150 mW/m-K. These conductivity values were then compared to the conductivity values calculated from the bed density in each panel and interpolations of conductivity data for aerogel beds across a range of compression using the hot-wire transient test method. Table 2.1 below provides a summary of this data.

Test Number	1	2	3	4	5
Truss Volume Fraction	0%	0%	0%	3.5%	3.4%
Aerogel Bed Density [kg/m^3]	64.2	80.4	91.3	61.4	78.0
LaserComp: Whole Panel Conductivity [mW/m-K]	26.7	25.1	23.4	31.9	26.5
LaserComp: Aerogel Bed Conductivity [mW/m-K]:					
- With polystyrene at 112 mW/m-K	22.3	20.8	19.4	25.8	21.2
- With polystyrene at 150 mW/m-K	22.0	20.6	19.2	24.7	20.3
Hot-Wire: Aerogel Bed Conductivity [mW/m-K]	23.7	20.0	18.0	24.4	20.5

Table 2.1: Comparison of compression testing results between hot-plate and hot-wire methods.

LaserComp testing was also done to evaluate the aerogel compression and truss adhesion methods. When compressing a bed of granules, there is a degree of spring-back when the compression force is released. Kevin Chen tested two compression methods that produced similar reductions in spring-back: holding the bed under compression for an hour or cycling between full and no compression ten times over about 10-15 minutes.[18] LaserComp test results from panels constructed using each compression method provided similar conductivity results. Therefore, all future panels were made using the cycling method in order to save time. For the panels with an internal truss, the truss needed to be epoxied to the inside of the panel faces. Again, Kevin Chen tested two methods to apply this epoxy to the inside of each panel face: spot gluing at each contact point or applying a continuous layer across the entire face. The spot-gluing method was problematic as it was challenging to apply the epoxy to all 162 contact points on a single face and affixing it to the truss before the epoxy had begun to set. Both methods produced similar LaserComp test results and therefore all future panels were made using a continuous layer of epoxy in order to save time.

2.6 Thermal Conductivity Testing – Concurrent Research

In addition to these thermal conductivity tests, a number of experiments were performed by Kevin Chen to physically characterize the aerogel granules.[18] Of particular interest were two experiments done by Chen to evaluate the physical impacts of compacting a bed of aerogel granules. The first set of tests performed were micro-computed tomography (micro-CT) in order to observe the change in the macroscopic, intergranular voids in the aerogel bed. The second set of tests was gas absorption/desorption, which was used to determine the microscopic pore size distribution within the granules themselves. As with the LaserComp testing, these experiments were all performed with the Cabot granules due to limitations in the availability of sufficient volumes of MIT samples.

In micro-CT, a sample is scanned with an x-ray beam which is used to develop a three dimensional density map of the sample. The map is then viewed as grayscale images of planar cross-section slices through the sample. Darker shades correspond to lower density materials; lighter colors to higher densities. Therefore, if two materials have similar densities, it may be difficult to distinguish between them in the micro-CT grayscale images. Since the Cabot granules have a density close to that of air (120-180 kg/m^3 compared to 128 kg/m^3, respectively), the samples were immersed in water (with a density of 1,000 kg/m^3) to provide the necessary contrast.[6] It was assumed that replacing the air with water would not significantly impact the void distribution during compression.

The samples were put in closed-off syringes, which were then compressed to the desired level. Excess water was allowed to flow out of the syringe through a filter so as to avoid any build-up of pressure that could damage the aerogel granules, which would in turn affect the results. The samples were then tested using a GE eXplore CT 120 system at the David H. Koch Institute for Integrative Cancer Research at MIT. Figure 2.9 below shows a representative set of scans from a range of different compression levels tested.

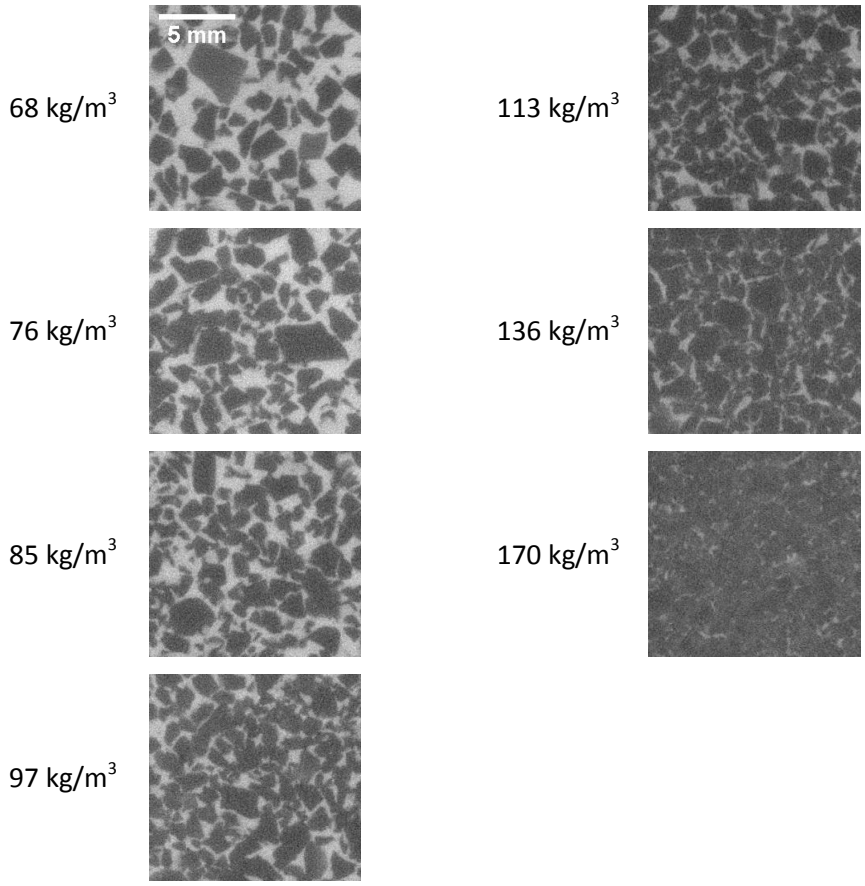

Figure 2.9: Micro-CT scans of aerogel granules (dark color) immersed in water (light color). Granular bed densities (in air) for each test are listed.[18]

These micro-CT scans were then analyzed using ImageJ – an image-processing software developed at the National Institute of Health (NIH) – in order to calculate the volume fraction of interstitial voids present at each compression level. At the lower compression levels, the grayscale histogram of the image provided a clear distinction between the aerogel portions of the image and the water-filled interstitial spaces. At higher compression levels, however, this distinction became less clear.

Therefore, the water-filled voids had to be identified using a more manual and visual process to adjust the grayscale threshold used by the software to calculate the area fraction in the image. Knowing the chamber volume, the void volume fraction and the mass of granules, one could also calculate an approximate density for the granules themselves. These results indicated that at higher compression levels, the granules appeared to have densified, presumably due to collapsing of their microstructure. However, there was an initial drop in the calculated granule density between the bed densities of 68 and 85 kg/m^3; this is most likely an artifact of measurement error from the image analysis – as there is no obvious physical reason for the granules to decrease in density at higher compressions – though such measurement error could not be readily quantified. The results from this image analysis are provided in Figure 2.10. This analysis focused on void fraction and did not include any quantification of void size distribution, which should be considered for future research.

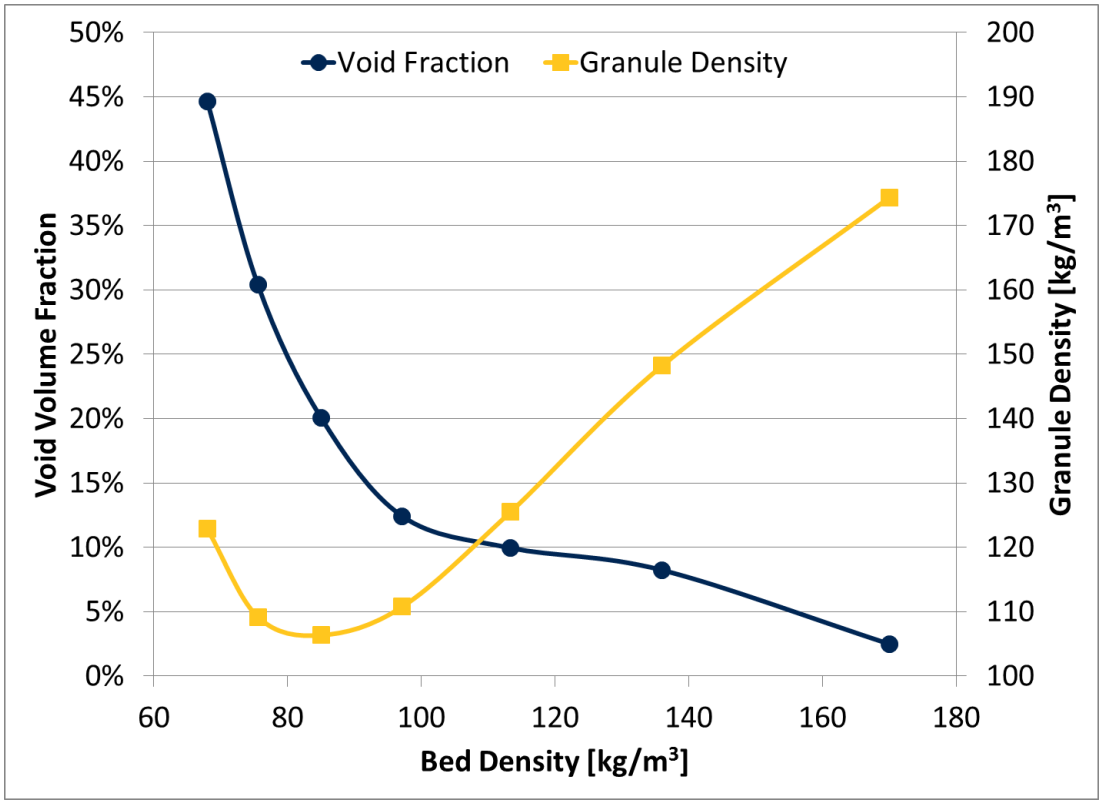

Figure 2.10: Micro-CT results of volume fraction of inter-granular voids for compressed Cabot aerogel granules.[18]

The second set of physical characterization tests performed on the Cabot granules was gas adsorption/desorption. In this technique, a small sample of material is placed in a glass reservoir which is initially evacuated and heated for a number of hours to drive off contaminants, such as water. Once this preparation step is complete, the sample is cooled (typically with liquid nitrogen), once again under vacuum, and then the appropriate analysis gas (nitrogen, in this case) is slowly bled into the reservoir to increase the pressure by small increments. As the pressure increases, the gas molecules will accumulate on the surface and seep into the pores of the sample. Continuing to increase the pressure will cause the gas to condense, starting in the smallest pores. Once complete saturation is reached, the gas pressure is incrementally reduced until all of the adsorbed gas has been evaporated from the sample. Following the Barrett, Joyner and Halenda (BJH) method, data from the adsorption and desorption cycles can then be evaluated to identify information about the pore size distribution of the sample.[28] Results from the gas sorption testing are provided in Figure 2.11. This testing showed that the total pore volume was not changed significantly until the samples exceeded a bed density of about 110 kg/m^3, at which point the pore volume results showed a clear decrease with increasing bed density.

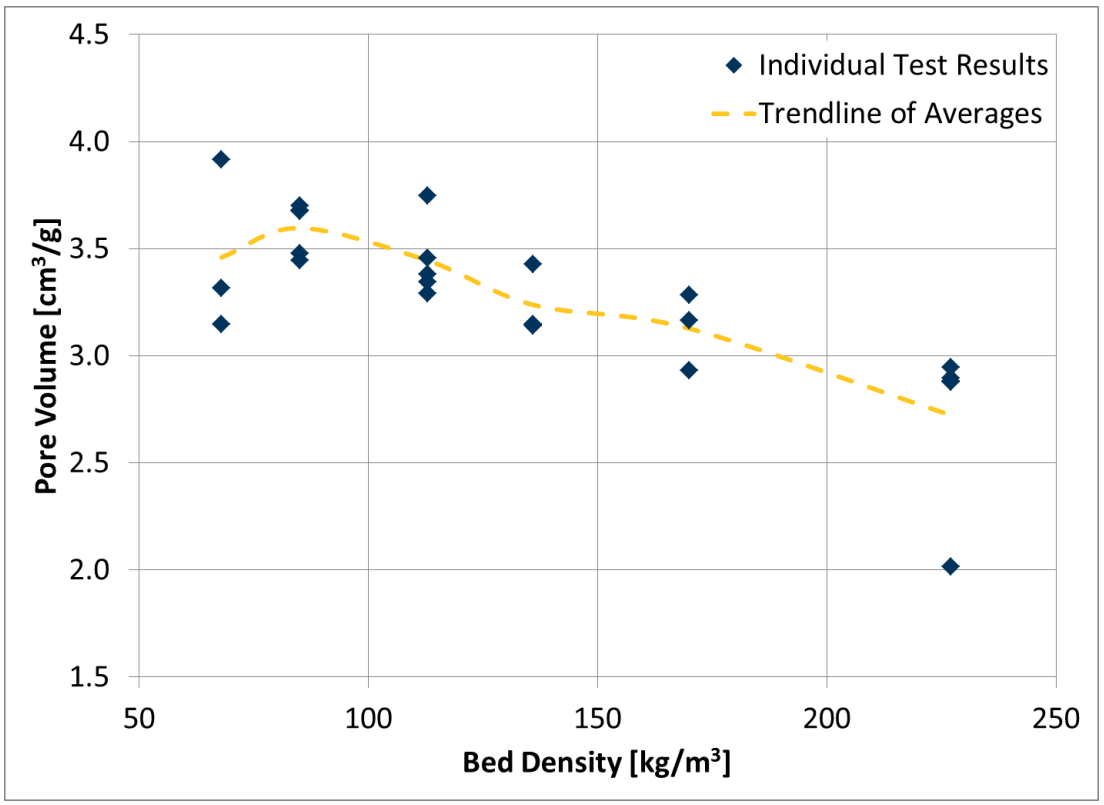

Figure 2.11: Pore volume calculations from gas sorption testing of compressed Cabot aerogel granules.[18]

2.7 Discussion of Thermal Conductivity Results

There are a number of observations that can be made from the hot-wire results including: the performance of aerogel beds under compression, the performance of aerogel beds under compression and vacuum and the relative performance of MIT aerogel granules compared to commercially available granules.

Compressing a bed of aerogel granules would have two main effects: shrinking the intergranular air-filled voids and collapsing the microstructure within individual granules. The former mechanism would decrease the thermal conductivity of the bed because the air in the voids should have a higher thermal conductivity than the individual aerogel granules (25 mW/m-K for air versus about 10-15 mW/m-K for bulk aerogel); the latter mechanism would increase the thermal conductivity of the granules (and by extension the granule bed) because these aerogels derive their low thermal conductivity from their low-density, nanoporous structure (see Chapter 1.1).[3][11] The micro-CT results (see Figure 2.10) show that the volume fraction of air in the granule bed was decreased by more than two thirds when it was compressed from 68 kg/m^3 to 97 kg/m^3. Meanwhile, the gas sorption results indicate that there is negligible impact on pore volume until the bed density exceeded about 110 kg/m^3. Combining this information, it could be expected that the thermal conductivity of a loosely packed bed of aerogel granules would initially decrease under compression before bottoming out and eventually increasing again at higher compression levels (see Figure 2.12). The hot-wire results for the Cabot granules appear to demonstrate this hypothesis (see Figure 2.4). The Cabot samples showed a minimum thermal conductivity of about 13 mW/m-K at about 150 kg/m^3, which is in the density range of the material itself (as specified in Cabot's documentation).[6]

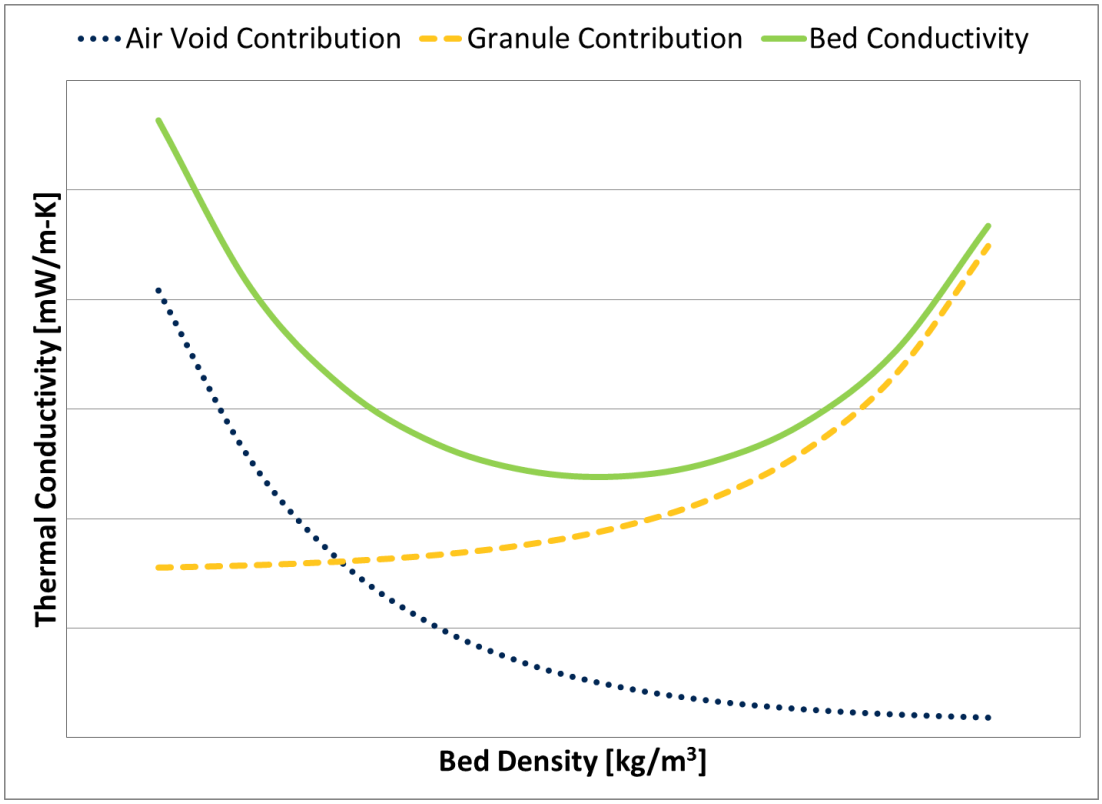

Figure 2.12: Qualitative visualization of contributing factors to granule bed conductivity.

Another major finding from these results is that the MIT granules were able to obtain similar conductivity results though at lower bed densities (about 20-30 kg/m^3 less). This would be of interest for the economics of such an insulation product, as this would mean decreased material costs for the same thermal performance.

Finally, the results from the vacuum chamber (see Figure 2.5) corroborated previous findings that the shape of the conductivity versus air pressure curve for beds of aerogel granules are different than those of monolithic aerogel samples. Where the monolithic samples drop off dramatically at relatively high pressures and then slowly level off, the granular curves dropped off less at first and then plateaued slightly before dropping off again at lower pressures. Also, compressing the aerogel granules caused the plateau effect with the granular samples to decrease so that the curve appeared more like that of the monolithic samples. These vacuum chamber results also indicated that the MIT granules were able to achieve similar results to the Cabot granules but at bed densities about 20 kg/m^3 lower.

The LaserComp testing provided some valuable comparison between experimental results and expected values for three distinct items: the conductivity of the polystyrene sheets, the contribution to

conductivity from the truss design and the conductivity of the aerogel granules. The expected values for each item came from three separate sources: literature values, theoretical calculations and previous hot-wire experiments, respectively.

As discussed in Chapter 2.4, there was uncertainty in the thermal conductivity of the polystyrene sheets, which were used to make the panel faces and trusses. A stack of five polystyrene sheets tested in the LaserComp system gave a conductivity of 112 mW/m-K. Unfortunately, attempts to remove the impacts of contact resistances per the LaserComp methodology for thin materials were unsuccessful. Therefore, analysis of the LaserComp results includes some additional uncertainty because of the uncertainty in the conductivity of the polystyrene components.

During the original development of the truss design and material selection for the panel system, Thomas Goutierre designed the truss system so that it would increase the conductivity of the panel core by no more than 2 mW/m-K, which assumed a thermal conductivity of 126 mW/m-K for the truss material; in other words, the term k_t' (see Equation 2.14) should not exceed 2 mW/m-K.[17] To evaluate this experimentally, the LaserComp data for the panels with a truss (see Table 2.1, tests 4 and 5) were compared to results from panels with similar bed densities but without a truss (see Table 2.1, tests 1 and 2, respectively). After correcting for the difference in the bed densities between the panels, the conductivity contribution of the truss was calculated to be about 4.6 mW/m-K (according to tests 1 and 5) or 1.5 mW/m-K (according to tests 2 and 5).These values are not impacted significantly by the uncertainty in the polystyrene conductivity. The latter comparison fits within the previous analytical expectations. The former comparison, however, is over twice the predicted value. The reason for such a discrepancy between these two comparisons is currently unknown and will require additional testing to definitively determine. The final comparison provided by the LaserComp data was for the measured conductivity of the aerogel granules. Separate conductivity measurements had been completed on compressed granule beds using the transient hot-wire method. One shortcoming of the hot-wire method for silica aerogel is that it underestimates the impacts of radiative heat transfer as compared to other, large scale test methods, such as the steady-state hot-plate method. The reason behind this is that the aerogel is relatively transparent to long-wave radiation for the timescales used in the hot-wire method. It was previously calculated by Ellann Cohen that the hot-wire method may underestimate thermal conductivity up to 3.3 mW/m-K.[3] The calculated aerogel conductivities based on the LaserComp results were all within this margin compared to the expected aerogel conductivities from the hot-wire results except for test 5 (when derived assuming the high polystyrene conductivity) and test 1

at either polystyrene conductivity (see Table 2.1); these tests had LaserComp results lower than the hot-wire expectations. The reason for this unexpected result is currently unclear. It may indicate that the higher conductivity value assumed for polystyrene is too high, though that cannot be definitively determined from these results and still does not resolve the issue with test 1.

There are a number of potential sources of error in these calculations. One such source could be in the manufacturing of the trusses. The truss pieces are currently made with a laser cutter and it creates some imperfections along the cut edges. However, water displacement measurements were performed on some truss pieces and they were consistently measured to be within 5% of the predicted volume according to the CAD files used to create the trusses. Some of the assumptions made in the theoretical calculation may also need to be reviewed. For example, it was assumed for the purposes of the calculations that heat traveling through the core travels separately through the aerogel and the truss, as if they were completely in parallel with each other. However, in reality it is likely that some amount of heat traveling through the low-conductivity aerogel would transfer to the relatively high-conductivity truss; this would increase the contribution to conductivity by the truss. This possibility has not been quantitatively reviewed. The calculations for the LaserComp results also assumed that the aerogel inside the panel was evenly distributed and compacted. When the truss was introduced, a grid was cut into the compression plate in order to fit around the truss; this grid was approximately 42% of the surface area of the compression plate. Calculations were done to see how the core conductivity would change if the aerogel was evenly compressed and if the aerogel was left completely uncompressed under the grid in the compression plate. For the (average) bed densities shown in Table 2.1, these two scenarios were within 1 mW/m-K of each other (with the homogenous compression scenario having the higher calculated conductivities). Also, since test 1 was involved in both of the discrepancies noted above, it is possible that some physical or tested measurement was incorrect. Though there is no way to know without repeating this test scenario.

3 LOW PRESSURE PANEL DESIGN

One performance metric that was analyzed in Chapter 2 was the thermal conductivity of aerogel granules at various air pressures. However, in order for these results to be relevant for a thermal insulation panel system, the panel design would need to be able to include a barrier material to reasonably maintain the internal vacuum over the life of the panel. Gas barrier systems are utilized across a range of industries: food and beverage packaging, medical supplies, electronics and industrial components. These systems are typically multi-layered thin films. The thickness (on the order of microns) and material selection (including various polymers, metals and metal oxides) of each layer are tailored for specific applications, with metal or metal oxide layers acting as the primary gas diffusion barriers in the system.[29] These are highly engineered films and therefore the development or even the specification of a barrier film design for our insulation panel system is outside the scope of this research effort. Instead, some specific film properties were evaluated, which could help guide the eventual barrier film selection process. The addition of a barrier film into the panel design will present a number of challenges – such as the increased material and production costs, durability concerns and thermal bridging potential – that need to be addressed.

This chapter will review the work done (including analyses and physical prototyping) to address the challenges presented by the addition of gas diffusion barrier systems.

3.1 Barrier Films – Impacts on Thermal Conduction

With vacuum insulated panel (VIP) systems, one must balance the need for low gas permeability with the need to minimize thermal bypass (a.k.a. thermal bridging) effects caused by the film. Any continuous and thermally conductive layers in a barrier film system will allow some heat to conduct around the edges of the panel, basically creating a thermal short that by-passes the low-conductivity core. In order to estimate the potential magnitude of such thermal bridging on the overall conductivity of the panel system, one can do some calculations using the basic rules of summing resistors in series and in parallel (see Equation 3.1 and Equation 3.2).

[Resistors In Series] $$R_{ser} = \sum R_i$$ Equation 3.1

[Resistors In Parallel] $$1/R_{par} = \sum(\emptyset_i/R_i)$$ Equation 3.2

Where:

R_{par} = Net resistance of i elements in parallel [m^2-K/W]

R_{ser} = Net resistance of i elements in series [m^2-K/W]

R_i = Resistance of the ith element [m^2-K/W]

$\emptyset_i$ = Cross-sectional area fraction of the ith element in parallel [unitless]

There are a number of models that can represent the basic set-up of an insulation panel fully wrapped in a barrier film. A lower boundary model would be to assume purely one dimensional heat flow through the system (see Figure 3.1); an upper boundary model would add the assumption that there is perfect transverse heat flow – i.e., a uniform temperature boundary – within each material (see Figure 3.2).

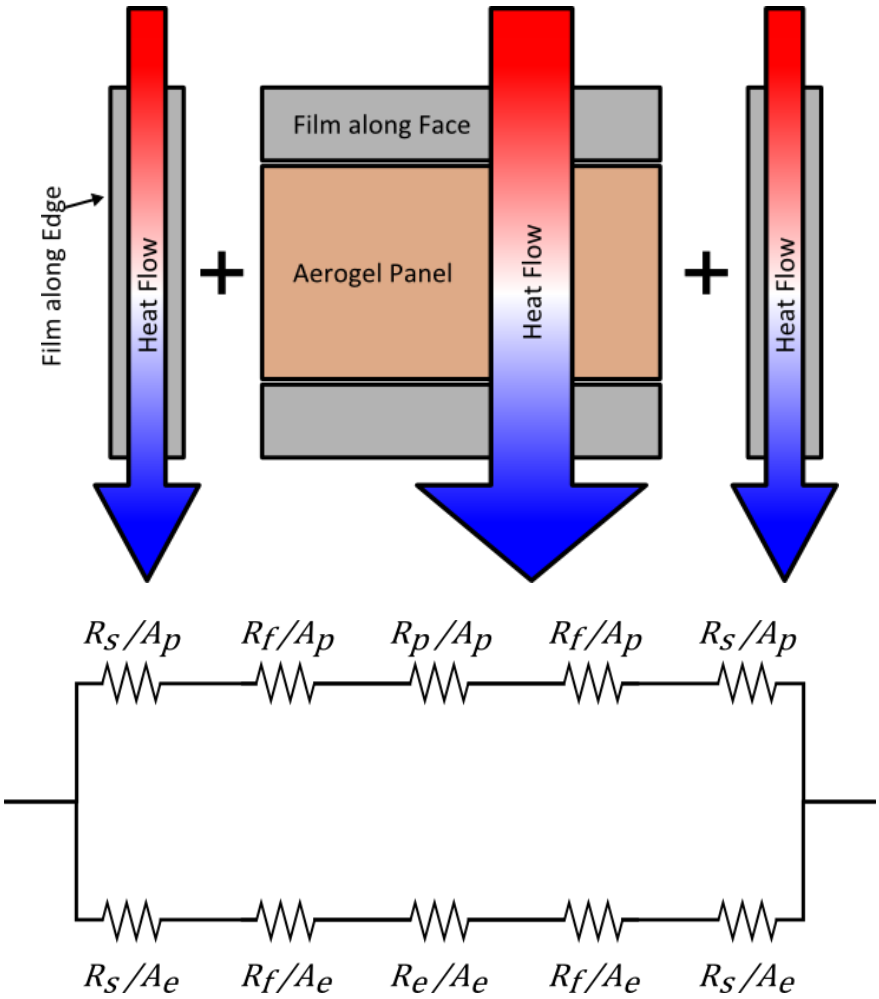

Figure 3.1: Schematic and circuit diagrams of 1D conduction through the panel.

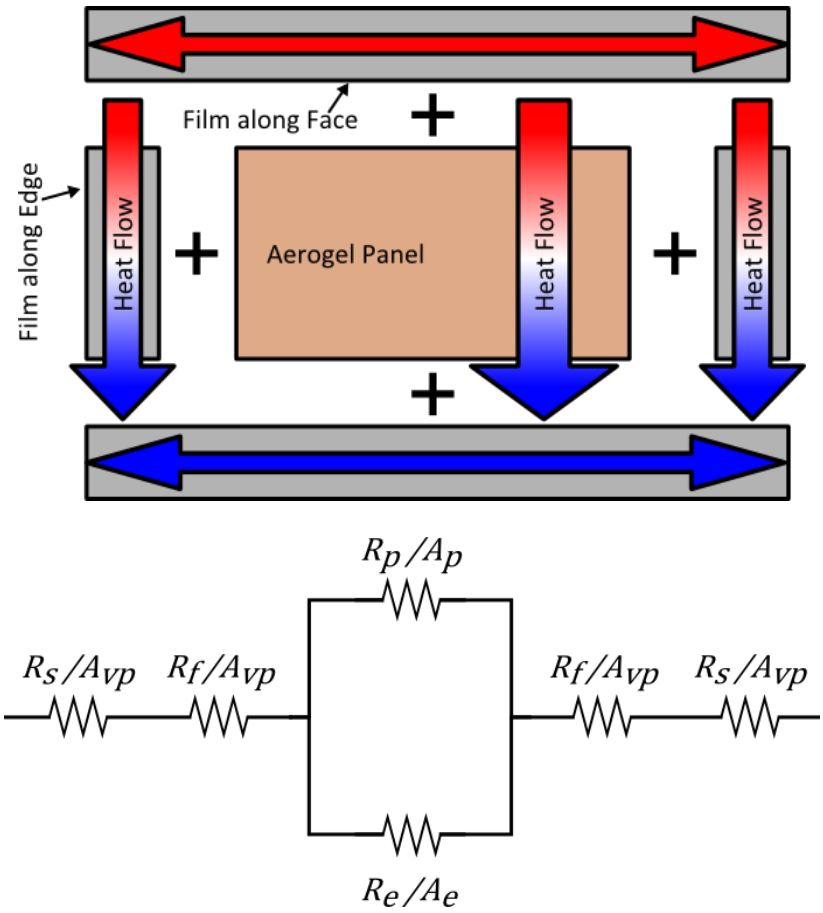

Figure 3.2: Schematic and circuit diagrams of 2D conduction through the panel.

Where:

A_e = Total cross-sectional area of the film along the edges, normal to the 1D heat flow [m^2]

A_p = Cross-sectional area of the panel (without film), normal to the 1D heat flow [m^2]

A_{vp} = Cross-sectional area of the vacuum panel (with film), normal to the 1D heat flow [m^2]

R_e = Resistance of the film along the edges, parallel to the 1D heat flow [m^2-K/W]

R_f = Resistance of the film along the face, parallel to the 1D heat flow [m^2-K/W]

R_p = Resistance of the core aerogel panel, parallel to the 1D heat flow [m^2-K/W]

R_s = Surface resistance from the panel to the surroundings [m^2-K/W]

Assuming:

$A_{vp} = A_p + A_e$

Through applications of Equation 3.1 and Equation 3.2, the effective total resistance for each model can be derived (see Equation 3.3 and Equation 3.4).

$$R_{eff}^{1D} = \left[\frac{\emptyset_c}{2R_f+R_p+2R_s} + \frac{\emptyset_e}{2R_f+R_e+2R_s}\right]^{-1}$$ Equation 3.3

$$R_{eff}^{2D} = 2R_f + \left[\frac{\emptyset_c}{R_p} + \frac{\emptyset_e}{R_e}\right]^{-1} + 2R_s$$ Equation 3.4

Where:

R_{eff}^{1D} = Net resistance of the panel system assuming 1D conduction only [m^2-K/W]

R_{eff}^{2D} = Net resistance of the panel system assuming complete 2D conduction [m^2-K/W]

$\emptyset_p$ = Cross-sectional area fraction of the core aerogel panel, normal to the 1D heat flow [unitless]

$\emptyset_e$ = Cross-sectional area fraction of the film along the edge, normal to the 1D heat flow [unitless]

Assuming:

$\emptyset_p$ = A_p/A_{vp}

$\emptyset_e$ = A_e/A_{vp}

Based on these analytical solutions, the one dimensional and two dimensional effective resistances were found to be within 10% of each other over the range of panel and film dimensions tested. Therefore, more complex heat flow models (such as the finite fin model) were deemed unnecessary for this analysis. A simple barrier film system (see Figure 3.3) was then used to explore the range of thermal bridging effects one could expect for a range of panel sizes and total thicknesses of the metalized layers within the barrier film (see Figure 3.4).[29] In order to minimize the thermal bridging affects, this system (like most current VIP barrier films) has a very thin metalized layer (less than 1 µm) and this layer is made of alumina, which has a relatively low thermal conductivity (10-40 W/m-K) compared to older barrier film materials (such as aluminum, which has a conductivity over 200 W/m-K).[30] For the purposes of the calculations, the surface resistances were assumed to be due to radiation and still air on both faces of the panel; different installation scenarios would therefore change these calculations.

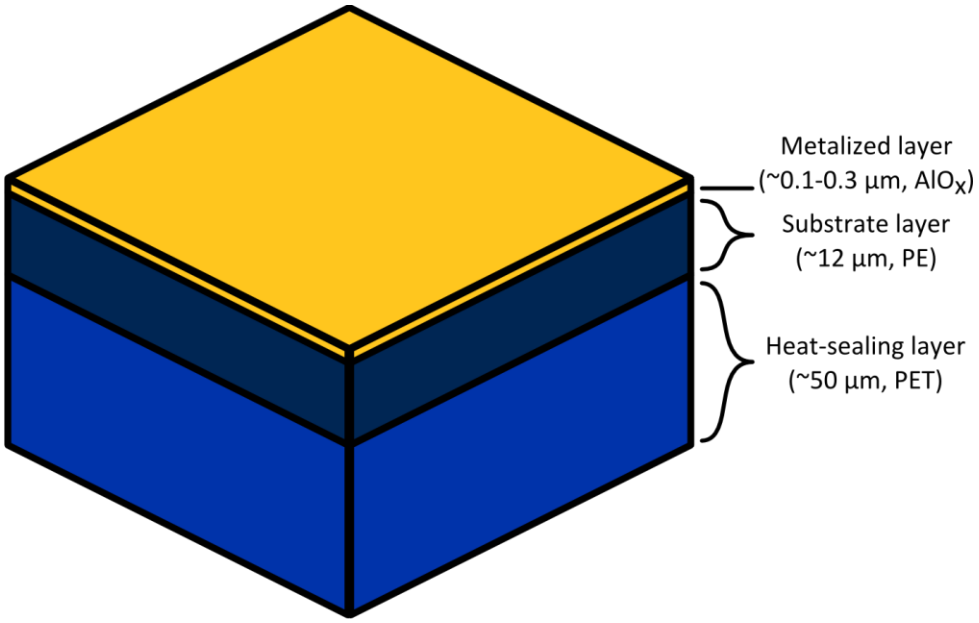

Figure 3.3: Composition of a simple barrier film system.[29]

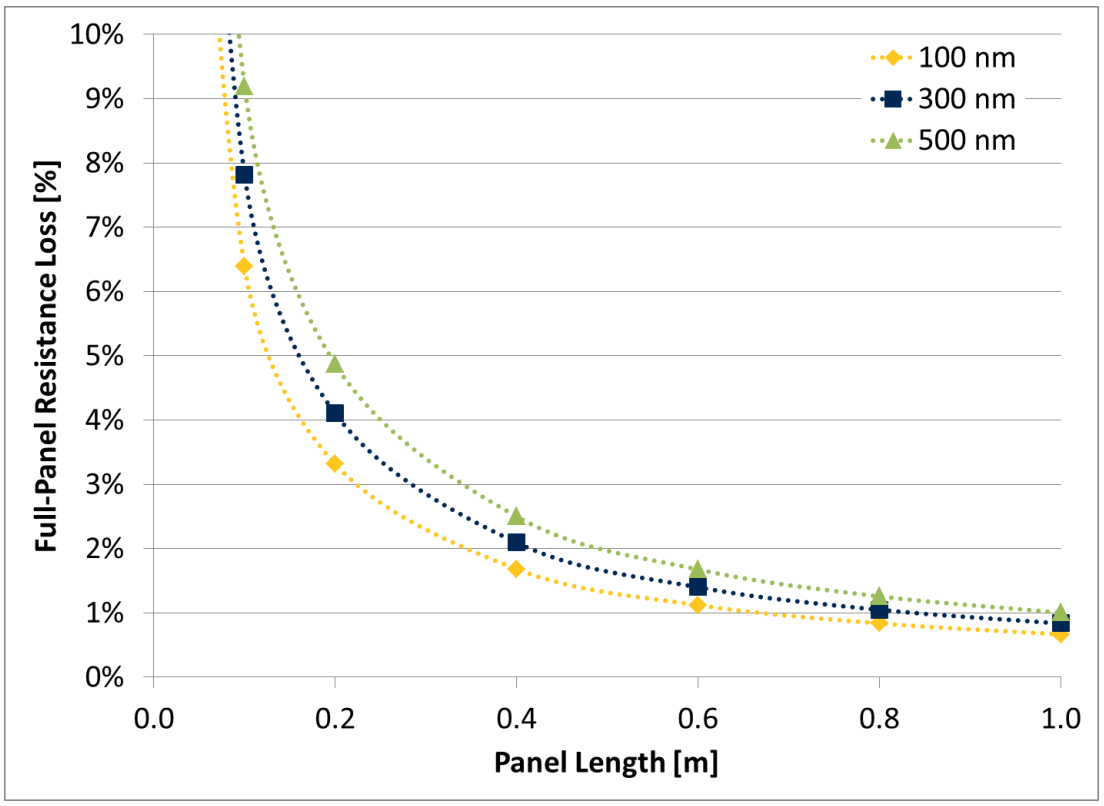

Figure 3.4: Calculated loss in whole-panel resistance values (including surface resistances) across a range of square panel lengths and total metalized layer thicknesses within the barrier film.

Assuming:

Panel thickness = 1.27 cm

Full panel conductivity (without barrier film) = 15 mW/m-K

Panel surface heat transfer value (convection plus radiation) = 10 W/m^2-K

Metalized layer conductivity = 40 W/m-K (worst-case value) [30]

Film substrate conductivity = 0.49 W/m-K (worst-case value) [31]

Heat-sealing layer conductivity = 0.4 W/m-K (worst-case value) [32]

Based on these design parameters and assumptions, the thermal bridging calculations demonstrate that barrier films can contain continuous alumina layers of thickness up to 500 nm without decreasing the whole-panel resistance by more than 10%. The metalized layers in VIP barrier films are typically 100 to 300 nm, so this initial analysis suggests that current barrier film systems may not create significant thermal bridging concerns.[33]

3.2 Barrier Films – Analysis of Diffusion

Having an approximate idea of the upper limit of metalized layer thickness that would be permissible without causing significant thermal bridging is critical to understand the maximum performance one could expect of the barrier film in terms of resistance to gas intrusion (and therefore loss of vacuum) over time. Using this knowledge, a simple analysis was performed to obtain an order-of-magnitude approximation for the maximum allowable gas transmission rates for the barrier film.

A volumetric flow rate across a film was found starting with an application of Fick's diffusion law and Henry's law of solubility (see Equation 3.5).[34][35] This volumetric flow rate can then be redefined using the ideal gas law (see Equation 3.6), assuming the environmental conditions the panel is exposed to don't deviate significantly from standard temperature and pressure (STP). Finally, these two equations can be combined to get the rate of change in internal pressure for a given pressure difference across a barrier film (see Equation 3.7). Note that this equation is in terms of only the panel design and film parameters. Also note that the internal volume term, V_{int}, is the effective volume of gas: in other words, it is the total internal volume of the panel minus the total volume occupied by any solid material (such as the solid network of the aerogel). These equations are written generically and could be applied to specific gasses (e.g., nitrogen or oxygen) or gas mixtures (e.g., air).

$$\dot{V}_{stp} = \frac{PA}{L}(p_{amb} - p_{int}) = JA(p_{amb} - p_{int}) \quad \text{Equation 3.5}$$

$$\dot{V}_{stp} = \frac{d}{dt}\left(\frac{nRT_{stp}}{p_{stp}}\right) = \left(\frac{T_{stp}}{p_{stp}}\right)\frac{d}{dt}\left(\frac{p_{int}V_{int}}{T_{int}}\right) = \left(\frac{T_{stp}V_{int}}{T_{int}p_{stp}}\right)\frac{d}{dt}p_{int} \quad \text{Equation 3.6}$$

$$\frac{d}{dt}p_{int} \equiv \dot{p} = JA\left(\frac{T_{int}p_{stp}}{T_{stp}V_{int}}\right)(p_{amb} - p_{int}) \quad \text{Equation 3.7}$$

Where:

- A = Surface area of the film [m^2]
- dt = Increment of time for gas diffusion [day]
- J = Gas transmission rate across the film [$(cm^3)_{STP}/m^2$-day-atm]
- L = Thickness of the film [m]
- n = Moles of gas [mol]
- $\dot{p}$ = Rate of internal (partial) pressure increase [atm/day]
- p_{amb} = Ambient (partial) pressure [atm]
- p_{int} = Internal (partial) pressure [atm]
- p_{stp} = Standard (partial) pressure ≡ 0.986 (for air) [atm]
- P = Permeability coefficient of the film material for a given gas [$(cm^3)_{STP}$/m-day-atm]
- R = Ideal gas constant ≡ 8.206×10^{-5} [m^3-atm/mol-K]
- T_{int} = Internal temperature of the panel [K]
- T_{stp} = Standard temperature ≡ 273.15 [K]
- V_{int} = Effective volume of gas inside the panel [m^3]
- $\dot{V}_{stp}$ = Volumetric flow rate across the film, at STP [$(cm^3)_{STP}$/day]

Assuming:

- J ≡ $\frac{P}{L}$

Equation 3.7 is an instantaneous rate of (partial) pressure change for a given (partial) pressure difference, which will change over time as gas gradually diffuses through the barrier film. Therefore this equation must be integrated over the life of the panel system. First, the variables of integration must be separated (see Equation 3.8) and the pressure integrand must be revised (see Equation 3.9) before both sides can be integrated (see Equation 3.10) and the transmission rate can be solved for (see Equation 3.11), which will be based on an assumed final panel pressure and the initial evacuated pressure.

$$\frac{dp_{int}}{p_{amb}-p_{int}} = JA\left(\frac{T_{int}p_{stp}}{T_{stp}V_{int}}\right)dt$$ Equation 3.8

$$\frac{dp_{int}}{p_{amb}-p_{int}} \rightarrow -\frac{d(p_{amb}-p_{int})}{p_{amb}-p_{int}}$$ Equation 3.9

$$ln\left(\frac{p_{amb}-p_o}{p_{amb}-p_f}\right) = JA\left(\frac{T_{int}p_{stp}}{T_{stp}V_{int}}\right)t_p$$ Equation 3.10

$$J = \left(\frac{T_{stp}V_{int}}{At_pT_{int}p_{stp}}\right)ln\left(\frac{p_{amb}-p_o}{p_{amb}-p_f}\right)$$ Equation 3.11

Where:

p_f = Final internal (partial) pressure (or internal (partial) pressure at "failure") [atm]

p_o = Original internal (partial) pressure [atm]

t_p = Panel lifetime [day]

Using the gas transmission rate from Equation 3.11, one can also calculate the mass transmission rate for the film (see Equation 3.12).

$$\dot{m}_p \equiv \rho J$$ Equation 3.12

Where:

$\dot{m}_p$ = Mass transmission rate across the film [g/m^2-day-atm]

ρ = Gas density at ambient temperature and pressure [g/m^3]

Permeability coefficients (or transmission rates) for a film will be different for different gas molecules and therefore these calculations need to be done for each molecular constituent. For the case of air, gas transmission rates are typically calculated for nitrogen and oxygen (which together represent about 99% of the air by volume: 21.0% is oxygen and 78.1% is nitrogen).[36] One rule of thumb is that the oxygen permeability for a given materials is typically about three to four times its nitrogen permeability.[37] Based this approximation, the transmission rates for oxygen and nitrogen can be calculated by assuming the total rate of change of the internal pressure (see Equation 3.7) is simply the sum of the rate of change of the internal partial pressures of oxygen and nitrogen. This also assumes that the thermal conductivity of the air inside the panel is dependent only on the internal pressure and is not affected by the gas mixture within the panel. For the purposes of this analysis, these assumptions

were deemed acceptable though they would need to be revisited for more rigorous studies. Table 3.1 below shows the maximum allowable performance values for the barrier film for the panel design discussed in this research. These calculations used an initial pressure of 0.001 atm (the initial pressure does not have a significant impact on the results below about 0.01 atm) and a final pressure of 0.2 atm (around the pressure where the granular beds started showing a faster rate of conductivity increase, according to Figure 2.5).

Constituent	Air	Nitrogen	Oxygen
Gas Transmission Rate [$(cm^3)_{STP}$ /m^2-day-atm]	1.06×10^{-1}	1.39×10^{-1}	4.86×10^{-1}
Mass Transmission Rate [g/m^2-day-atm]	1.26×10^{-4}	1.59×10^{-4}	6.36×10^{-4}
(Partial) Pressure Change Rate [atm/day]	2.03×10^{-5}	1.62×10^{-5}	4.09×10^{-6}

Table 3.1: Calculated barrier film performance requirements.

Assuming:

Panel thickness = 1.27 cm

Square panel length = 20 cm

Initial internal pressure = 0.001 atm

Final (at failure) internal pressure = 0.2 atm

Time to failure = 30 years

Internal temperature = 298 K

Internal air volume ratio = 99.98%

These performance values are in the range of those seen for typical films used for vacuum insulation panels. The most commonly listed performance value for barrier films used for VIP systems, oxygen transmission rates, is typically on the order of 0.1 $(cm^3)_{STP}/m^2$-day-atm.[29][33] These calculations have limited applicability due to a number of reasons including: (1) transmission rates will increase at higher temperatures and/or humidities, (2) the barrier films are installed using more complex geometries than the simple case used for the calculations and (3) various aging effects on the film can cause its diffusion properties to change over time.[38][39] However, this exercise still provided some order-of-magnitude estimations for necessary film performance, which can help guide future research.

3.3 Barrier Films – Design Considerations

The barrier film is designed to not only achieve the required vacuum level for the insulation panel, but also to maintain it below a certain maximum internal pressure over the life of the system. This, however, assumes that the barrier film remains intact throughout this lifetime. Any cut or puncture in the film would effectively result in premature failure of the insulation system. Therefore, vacuum insulation panel systems often require careful handling and may be installed with additional layers to provide physical protection against accidental nicks and scratches. The insulation panels being developed at MIT are envisioned to potentially serve as building insulation, an industry in which the panels would likely be exposed to more wear and tear through rougher handing during transportation and installation. Therefore, another aspect of the barrier film that was considered was how to integrate it with the panel while providing some additional physical protection for the film.

Barrier films typically represent the complete external surface of vacuum insulation panels (see Figure 3.5a). A significant concern with this design is that it exposes the whole film surface. Two potential alternatives were posited in order to reduce this exposure. The first was to move the film inside of the panel faces (see Figure 3.5b); the main downside of this option is that it may weaken the mechanical connection between the truss and the internal surfaces of the panel faces. The second alternative was to sandwich the barrier film between a pair of face pieces on either side (see Figure 3.5c); this could increase the material requirements for the panels and could decrease the effective insulation value per centimeter of thickness of the panel system.

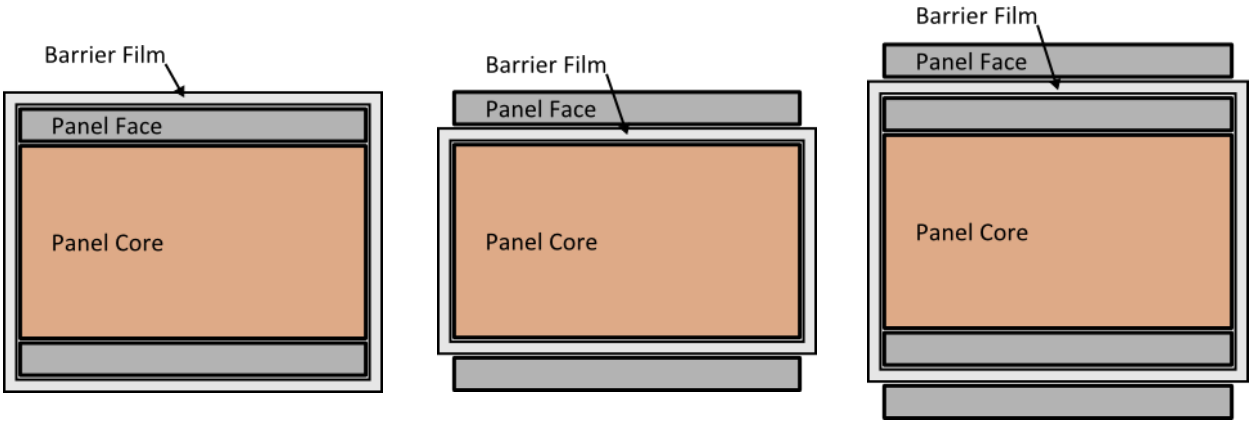

(a) Outside **(b) Inside** **(c) Sandwiched**

Figure 3.5: Typical barrier film installation (a) for a vacuum panel and two alternatives: installing the film inside the panel faces (b) and sandwiching the film between two face pieces (c).

3.4 Barrier Films – Design Prototyping

The internal film option (see Figure 3.5b) was selected for physical prototyping. The first step taken was to develop a design or shape in which to cut the barrier film. The main goal of this step was to reduce the required length of seams in the film that would ultimately need to be sealed since seams are a potential point of weakness in any barrier film. A single, two-dimensional T-shaped piece of film (see top of Figure 3.6) would have three seams along the panel edges and four along the panel corners. It would also be possible to seal all but one edge and the two adjacent corner seams of the film prior to installation into the panel (see bottom of Figure 3.6).

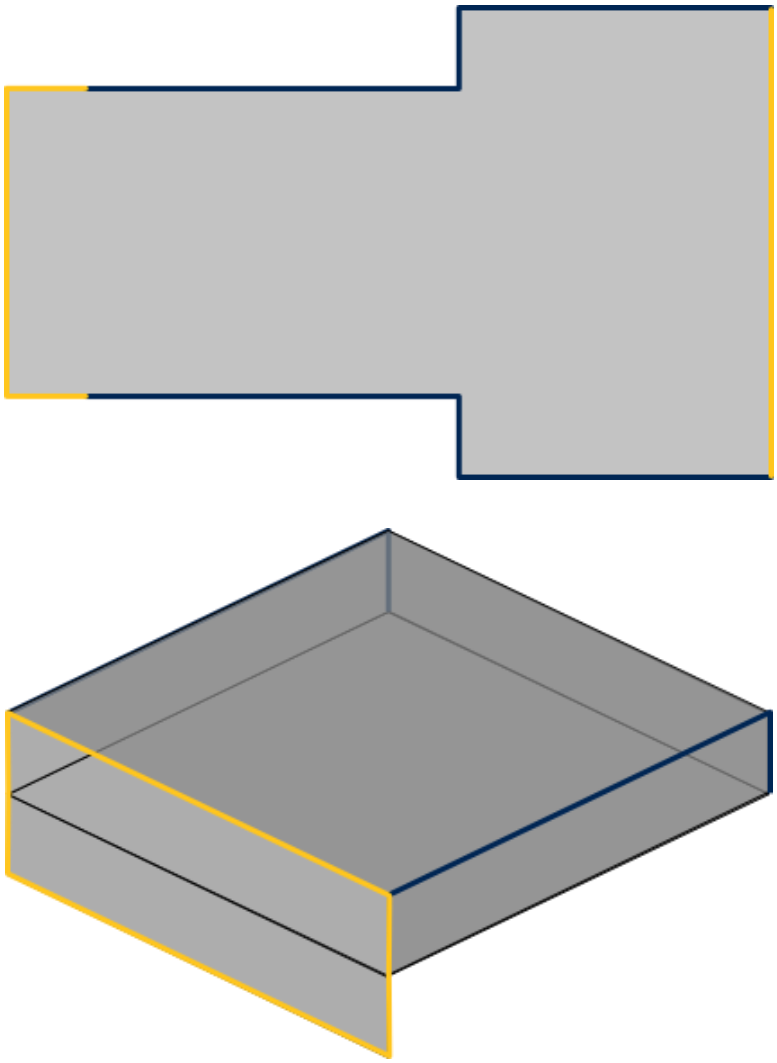

Figure 3.6: Schematic of the barrier film design with pre-installation seams highlighted in blue and post-installation seams in gold. (Top) Shape of a single barrier film piece. (Bottom) Barrier film piece prepared for installation into panel.

The next goal of the prototyping was to find a method by which this internal film concept could be incorporated into the flexible panel design that was previously developed by Ellann Cohen. In this design concept, each panel would be made up of a number of interlocked triangular sub-panels. Figure 3.7 shows a prototype made by Cohen of this flexible design with Figure 3.8 providing a schematic of the sub-panel joint design.[3]

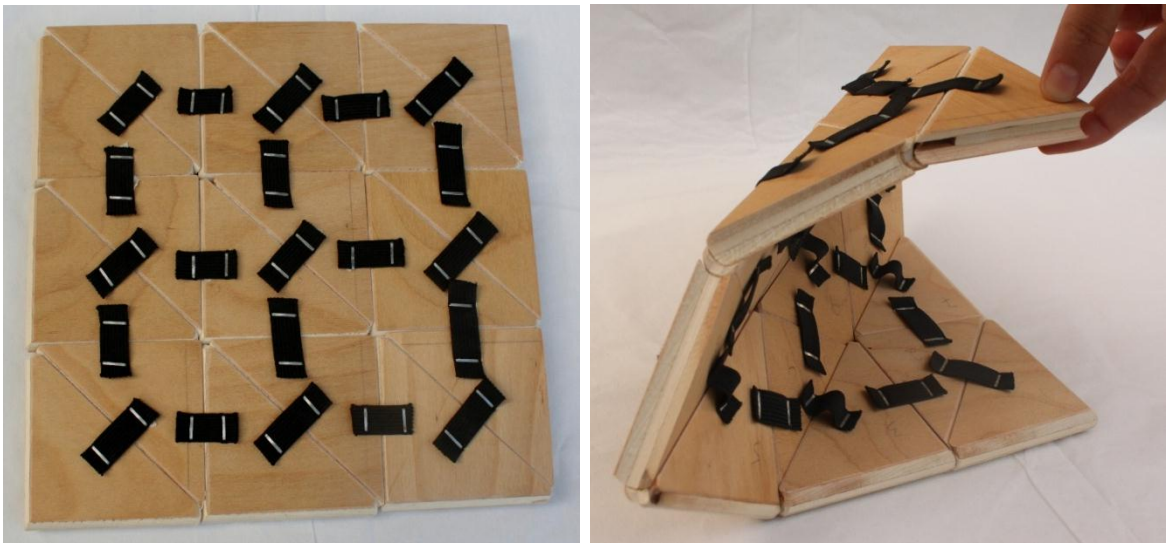

Figure 3.7: Wooden prototype for a flexible panel design developed by Ellann Cohen.[3]

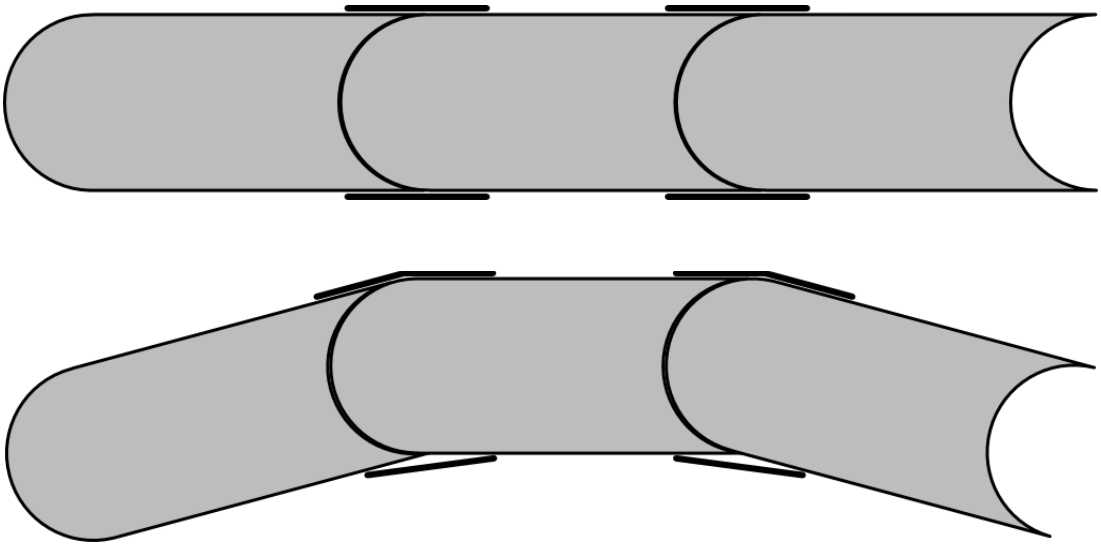

Figure 3.8: Schematic of sub-panel joints when straight (top) and flexed (bottom).[3]

This interlocking sub-panel edge design allows for the formation of a flexible joint with high thermal resistance. To create the concave and convex sub-panel edges, it was proposed that the film would be flexed slightly inwards (creating a concave surface along each edge) and then "filled" with a bead of spray foam insulation (see top of Figure 3.9). The concave and convex edges could then be cut from the foam along each edge, leaving the barrier film intact (see bottom of Figure 3.9).

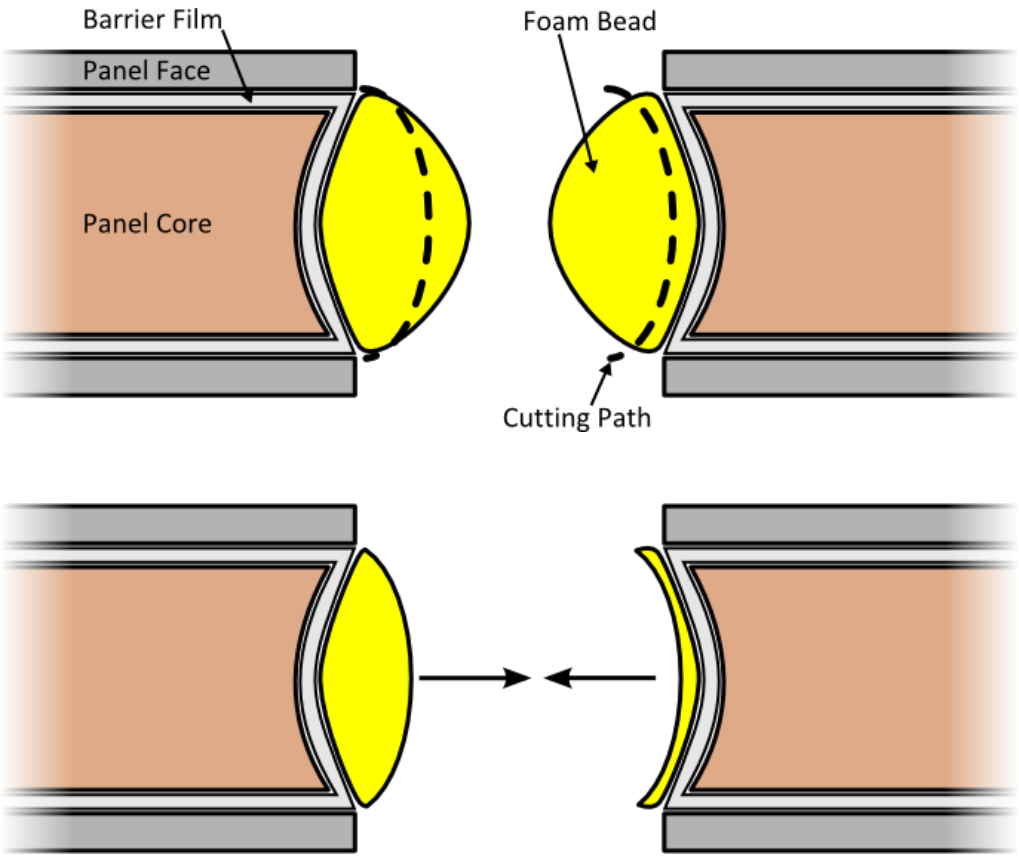

Figure 3.9: Potential sub-panel joint construction using a foam bead to act as the interface. Schematic with the full bead (top) and after cutting to the desired concave/convex shape (bottom).

One problem that was found with this design was that the film seams at the panel corners did not come together flatly. One potential solution would be to develop a more complex film shape (instead of the design shown in the top of Figure 3.6) that could resolve this geometric incompatibility. However, this would likely complicate the manufacturing process of the film and may require more seams to be sealed. A solution that resolved this incompatibility using the existing film shape was the

use of seams at each corner that can be folded into an S-shaped curve along the length of the corner (see Figure 3.10).

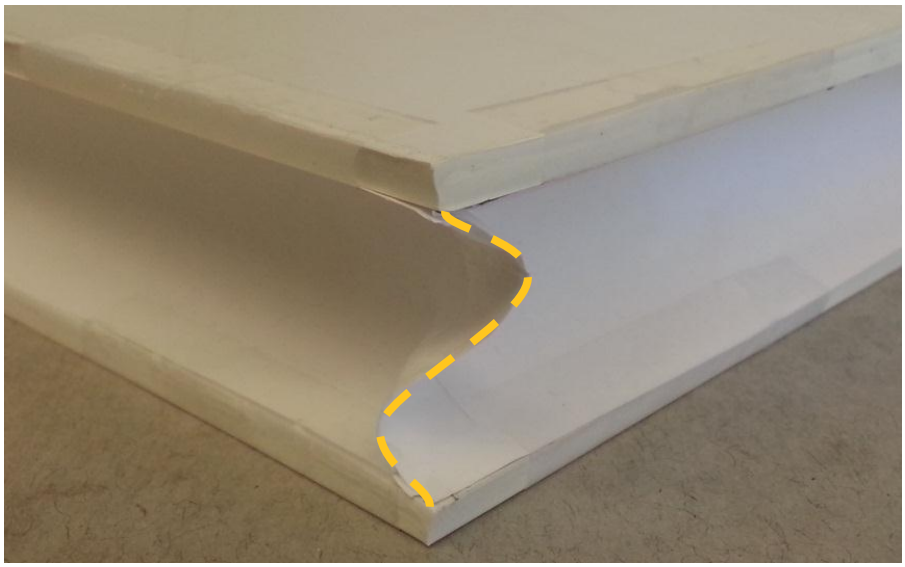

Figure 3.10: Prototype of a method to address geometric incompatibility of the film at each panel corner. The curve at the intersection has been highlighted in gold.

This physical prototyping exercise also highlighted the difficulty of installing the internal barrier film along with the internal truss. Unless this issue can be resolved, this internal film installation method will not be feasible. Either way, the feasibility of the other two film installation methods (see Figure 3.5a and Figure 3.5c) should be similarly explored with physical prototyping.

4 CONCLUSIONS AND FUTURE WORK

Aerogels show great promise for a variety of uses, including thermal insulation. However, the use of monolithic pieces of aerogel on the scale of typical building materials presents challenges in terms of manufacturing and product design:

- The synthesis process for aerogel requires molds and vessels that would need to be sized accordingly. The larger the individual aerogel pieces required, the larger the equipment needed.
- Aerogels shrink during the drying stage, even when processed carefully. This can cause complications when the aerogel is being dried inside of a composite structure (such as was proposed previously with the MIT panel design). It also requires the sol-gels to be slightly oversized compared to the desired final dimensions.
- The synthesis process includes multiple diffusion-limited steps. Larger, thicker pieces with lower surface area-to-volume ratios could dramatically increase the processing time and material costs (e.g., ethanol and carbon dioxide).
- Due to the inherent fragility of low-conductivity silica aerogel formulations, there is a significant risk that a large monolithic piece could be damaged (whether during manufacturing, transportation, installation and/or use), which could decrease the thermal performance of the system. A major design consideration therefore would have to be to minimize this risk of damage.

Based on these concerns regarding monolithic aerogels, the research at MIT was refocused towards granular aerogel samples. While going with granular samples addressed many of the concerns with monolithic samples, it brought up some new issues:

- Since the aerogel formulations being worked with have a lower thermal conductivity than air, a bed of aerogel granules will always have a higher conductivity than a monolithic piece of the same aerogel. Therefore, the granule bed will likely need to be compressed to minimize intergranular voids.
- Monolithic aerogel samples showed significant improvements in their thermal performance at modestly reduce air pressures; previous testing of aerogel granules, however, showed

only minimal improvements until much lower pressures were reached. Therefore, before a reduced-pressure, granule-filled panel was going to be considered, it would need to be demonstrated that such a system would not require such low pressures.

- Assuming the granules will need to be packed into the panel (rather than simply loose-filled), a method will need to be devised to assemble the panels in such a way that the granules are compressed as needed when installed.

4.1 Conclusions

The aerogel research at MIT continues to work towards demonstrating the feasibility of a new aerogel-based thermal insulation panel system. Over the last two years, this research has focused on addressing the above-listed concerns regarding granular aerogels. This research has demonstrated the thermal conductivity of aerogel granules using the hot-wire method across a range of compression for both a commercial product from Cabot and a formulation developed at MIT. Under compression, it was found that the granule bed appears to reach a minimum point in the range of the monolithic density of the aerogel itself. For Cabot (with a monolithic density in the range of 120-180 kg/m^3) this occurred around 150 kg/m^3 at 13 mW/m-K. The research was unable to reach a minimum point for the MIT granules, but the lowest conductivity recorded was 12 mW/m-K (monolithic samples of MIT aerogels were previously measured to be 10 mW/m-K at ambient conditions). Overall, the MIT granules were able to achieve similar conductivities as the Cabot granules, but at bed densities about 20-30 kg/m^3 lower; this indicates the potential for material (and therefore cost) savings if this product were to be commercialized.

The same Cabot and MIT granular samples were similarly tested inside of a vacuum chamber. Again the MIT granules appeared to achieve similar conductivity levels at bed densities 20 kg/m^3 lower than the Cabot samples. The granular samples showed an initial decrease in conductivity at small pressure drops, then an almost plateau in conductivity until the decreasing again below about 0.01 atm. At higher compression levels, however, the conductivity versus bed density curve began to more closely mimic the exponential shape seen with monolithic samples. For example, the curve for the MIT granular samples at 132 kg/m^3 looked similar to the MIT monolithic curve (150 kg/m^3), though at conductivities 2-3 mW/m-K higher.

Guarded hot-plate thermal conductivity testing was also performed on aerogel-filled panels using a LaserComp system. This testing provided some initial corroboration for previous analytical work.

It was previously determined by Ellann Cohen that the transient hot-wire tests should underestimate the contribution of radiative heat transfer through a sample compared to the steady-state hot-plate test by up to 3.3 mW/m-K. The thermal conductivities calculated from the LaserComp results were up to 1.5 mW/m-K greater than the corresponding hot-wire values. Thomas Goutierre designed the internal truss system to contribute no more than 2 mW/m-K to the conductivity of the panel core. Comparing two pairs of LaserComp results, this value was calculated at either 4.6 mW/m-K or 1.5 mW/m-K. Further testing will need to be done to resolve this discrepancy.

Finally, work was also done to address various design concerns with the panel system, specifically regarding the incorporation of a barrier film to support an internal vacuum. Analyses were done into the potential thermal bridging effects and gas diffusion rates based on current design parameters for the panel system. Based on a simple barrier film system, thermal bridging was found to decrease the whole-panel resistance by no more than 10%. The maximum allowable oxygen transmission rate that would still preserve sufficient internal vacuum over the life of the panel was calculated to be about 0.45 cc/m^2-day-atm; commercial barrier films used in VIP systems have rated oxygen transmission rates on the order of 0.1 cc/m^2-day-atm. While promising, these were only preliminary analytical estimates and they will need to be followed up with more robust analytical and experimental work. Physical prototyping of an internal film design highlighted a number of issues that must be addressed for the design to be feasible (such as how to minimize the number of seams to seal and how to provide the concave/convex edges needed for the flexible joint design while keeping the barrier film intact). Potential solutions were identified for most of these issues, but the main unresolved problem with this design is how the internal film will interact with the internal truss without compromising the integrity of the barrier film or the mechanical properties of the panel.

4.2 Future Work

Over the last two years, the research at MIT has progressed the development of a new, high-performance panelized aerogel insulation system as part of the DuPont-MIT Alliance. This work is far from over, however. Some necessary next steps and promising avenues of research include:

- Aerogel synthesis: Currently, the MIT granules are made manually from small monolithic samples. This is an imprecise and time-consuming process. It would be valuable to develop a method to synthesize the aerogel samples as granules. There are also a number of ways that

the synthesis process could be expedited, though it has not been verified which of these options can be implemented without negatively impacting the performance of the final aerogel product.

- Hot-wire testing: It would be valuable to obtain a full conductivity versus bed density curve for MIT granules past their minimum point and to continue the vacuum chamber testing across a broader range of bed densities and air pressures. The vacuum testing could also be done at different gas mixtures (to account for different diffusion rates of oxygen and nitrogen) to see if that impacts the overall conductivity.
- LaserComp testing: Additional testing is needed under new and previously-tested conditions in order to obtain a more robust data set with which to analyze the analytical expectations of the system. Also, it would be interesting to test a panel system with radiant barriers installed on the inside faces to observe the potential to reduce radiative heat transfer through the panel.
- Barrier film analyses: More robust analytical work needs to be done into the thermal bridging and gas diffusion behavior of relevant barrier film systems. Eventually, experimental work will be required.
- Panel design: Physical prototyping uncovered design problems and potential solutions that had not previously been identified. This work should continue, including exploring other film installation methods, in order to better transfer the laboratory results into a fully functional insulation product.

5 REFERENCES

[1] Architecture 2030, “Solution: The Building Sector.” [Online]. Available: http://architecture2030.org/the_solution/buildings_solution_how. [Accessed: 08-May-2013].

[2] D&R International, Ltd., “2011 Buildings Energy Data Book,” Mar. 2012.

[3] E. Cohen, “Thermal Properties of Advanced Aerogel Insulation,” Massachusetts Institute of Technology, 2011.

[4] R. T. Bynum, *Insulation Handbook*. New York: McGraw-Hill, 2001.

[5] Aspen Aerogel, “Aspen Aerogel Spaceloft Data Sheet.” [Online]. Available: http://www.aerogel.com/products/pdf/Spaceloft_DS.pdf. [Accessed: 08-May-2013].

[6] Cabot Corporation, “Data Sheet - Cabot aerogel particles.” [Online]. Available: http://www.cabot-corp.com/wcm/download/en-us/ae/Data%20Sheet%20Cabot%20Aerogel%20P100_200_300_400_4_2011_FINAL.pdf. [Accessed: 07-May-2013].

[7] Cabot Corporation, “Data Sheet - Cabot Thermal Wrap.” [Online]. Available: http://www.cabot-corp.com/wcm/download/en-us/ae/Data%20Sheet%20Thermal%20Wrap%20TW350_600_800_4_2011_FINAL.pdf. [Accessed: 09-May-2013].

[8] ThermoCor, “ThermoCor Vacuum Insulated Panels.” [Online]. Available: http://thermocorvip.com/vacuum-insulation-panels/. [Accessed: 09-May-2013].

[9] NanoPore, “NanoPore Vacuum Insulation Panels and Inserts.” [Online]. Available: http://www.nanopore.com/documents/NanoPore%20VIP.pdf. [Accessed: 09-May-2013].

[10] S. S. Kistler, “Coherent Expanded Aerogels and Jellies,” *Nature*, vol. 127, no. 3211, p. 741, May 1931.

[11] *Aerogels Handbook*. New York: Springer Science+Business Media, LLC, 2011.

[12] S. S. Kistler and A. G. Caldwell, “Thermal Conductivity of Silica Aerogel,” *Industrial & Engineering Chemistry*, vol. 26, no. 6, pp. 658–662, 1934.

[13] Aerogel.org, “What is Aerogel?” [Online]. Available: http://www.aerogel.org/?p=3. [Accessed: 09-May-2013].

[14] L. R. Glicksman, “Heat Transfer in Foams,” in *Low Density Cellular Plastics: Physical Basis of Behaviour*, 1st ed., London; New York: Chapman & Hall, 1994, pp. 104–152.

[15] Aerogel.org, “How is Aerogel Made?” [Online]. Available: http://www.aerogel.org/?p=4. [Accessed: 08-May-2013].

[16] Y. Zuo, “Preparation of Silica Aerogels with Improved Mechanical Properties and Extremely Low Thermal Conductivities through Modified Sol-Gel Process,” Massachusetts Institute of Technology, 2010.

[17] T. Goutierre, “Advanced Thermal Insulation for Energy Efficient Buildings: Structural Performance of Aerogel Composite Panels,” Massachusetts Institute of Technology, 2011.

[18] K. Chen, “Truss Core Sandwich Panels with Compacted Aerogel Insulation,” Massachusetts Institute of Technology, 2013.

[19] M. J. Assael, K. D. Antoniadis, and W. A. Wakeham, “Historical Evolution of the Transient Hot-Wire Technique,” *International Journal of Thermophysics*, vol. 31, no. 6, pp. 1051–1072, 2010.

[20] H. S. Carslaw, *Conduction of Heat in Solids*, 2nd ed. Oxford: New York: Clarendon Press; Oxford University Press, 1986.

[21] “LaserComp FOX304: Thermal Conductivity Instrument.” LaserComp, Inc.

[22] K. Collins (LaserComp), Email: “RE: Information request on FOX304 system,” 05-Jun-2012.

[23] McMaster-Carr, “More About Plastics,” 2012. [Online]. Available: http://www.mcmaster.com/#8574kac/=mrj9os. [Accessed: 15-May-2013].

[24] *Cambridge Engineering Selector*. Granta Design Limited, 1999.

[25] R. Weast, *Handbook of Chemistry and Physics*, 66th ed. Chemical Rubber Company, 1985.

[26] “Tests of thin samples stacked (using FOX50 instrument).” LaserComp, Inc., 23-Oct-2008.

[27] W. P. Lewis (Cabot), Email: “Fw: The following web inquiry has been sent to your attention,” 31-Jan-2012.

[28] Micromeritics Instrument Corporation, “Gas Adsorption Theory.” [Online]. Available: http://www.micromeritics.com/repository/files/gas_adsorption_theory_poster.pdf. [Accessed: 07-May-2013].

[29] “IB-Film General Brochure 2012.” Dai Nippon Printing Company, 21-Mar-2012.

[30] D. G. Cahill, S. M. Lee, and T. I. Selinder, “Thermal Conductivity of κ-Al2O3 and α-Al2O3 Wear-Resistant Coatings,” *Journal of Applied Physics*, vol. 83, no. 11, pp. 5783–5786, 1998.

[31] INEOS Olefins and Polymers USA, “Typical Engineering Properties of HDPE.pdf.” [Online]. Available: http://www.ineos.com/Global/Olefins%20and%20Polymers%20USA/Products/Technical%20information/Typical%20Engineering%20Properties%20of%20HDPE.pdf. [Accessed: 10-May-2013].

[32] “Polyethylene Terephthalate (Polyester, PET, PETP) Material Information.” [Online]. Available: http://www.goodfellow.com/E/Polyethylene-terephthalate.html. [Accessed: 13-May-2013].

[33] D. Kaczmarek, “Barrier films for vacuum insulation panels (VIP),” *7th International Vacuum Insulation Symposium*, p. 91, 2005.

[34] A. F. Mills, *Mass Transfer*. Upper Saddle River, N.J.: Prentice Hall, 2001.

[35] E. C. Suloff, “Sorption Behavior of an Aliphatic Series of Aldehydes in the Presence of Poly(ethylene terephthalate) Blends Containing Aldehyde Scavenging Agents,” 06-Dec-2002. [Online]. Available: http://scholar.lib.vt.edu/theses/available/etd-12042002-124439/. [Accessed: 14-Jun-2012].

[36] “Air Composition,” *The Engineering Toolbox*. [Online]. Available: http://www.engineeringtoolbox.com/air-composition-d_212.html. [Accessed: 13-May-2013].

[37] D. K. Murphy, “Are Nitrogen Molecules Really Larger Than Oxygen Molecules?” [Online]. Available: http://www.getnitrogen.org/pdf/graham.pdf. [Accessed: 09-May-2013].

[38] A. Binz and A. Moosmann, “Vacuum Insulation in the Building Sector: Systems and Applications,” *IEA/ECBCS Annex*, vol. 39, Dec. 2005.

[39] H. Simmler and S. Brunner, “Vacuum insulation panels for building application: Basic properties, aging mechanisms and service life,” *Energy and Buildings*, vol. 37, no. 11, pp. 1122–1131, Nov. 2005.

6 APPENDIX

Ammonium fluoride
Ammonium hydroxide
Deionized water
Ethanol
Hydrochloric acid
Tetraethyl orthosilicate

Table 6.1: List of chemicals used in synthesis of MIT aerogels.[16]

	MIT (16E)	Cabot (P100)	Cabot (TLD 302/P300)
Base Material	Silica		
Material Form	Monolithic or Granular	Granular	
Granule Size Distribution [mm]	[Varies]	0.01-4.0	1.2-4.0
Monolithic Density [kg/m^3]	150	120-180	
Monolithic Conductivity [mW/m-K]	9.5	[Undocumented]	
Granule Conductivity [mW/m-K]	[See Figure 2.4]		

Table 6.2: Material properties of MIT and Cabot aerogels.[3][6][27]